HHS Public Access

Author manuscript

Multiscale Model Simul. Author manuscript; available in PMC 2017 October 16.

Published in final edited form as:

Multiscale Model Simul. 2016 ; 14(2): 668–707. doi:10.1137/15M1013110.

MESOSCOPIC MODELING OF STOCHASTIC REACTION-DIFFUSION KINETICS IN THE SUBDIFFUSIVE REGIME

EMILIE BLANC, **STEFAN ENGBLOM**, **ANDREAS HELLANDER**, and **PER LÖTSTEDT**

Division of Scientific Computing, Department of Information Technology, Uppsala University, P. O. Box 337, SE-75105 Uppsala, Sweden

Abstract

Subdiffusion has been proposed as an explanation of various kinetic phenomena inside living cells. In order to fascilitate large-scale computational studies of subdiffusive chemical processes, we extend a recently suggested mesoscopic model of subdiffusion into an accurate and consistent reaction-subdiffusion computational framework. Two different possible models of chemical reaction are revealed and some basic dynamic properties are derived. In certain cases those mesoscopic models have a direct interpretation at the macroscopic level as fractional partial differential equations in a bounded time interval. Through analysis and numerical experiments we estimate the macroscopic effects of reactions under subdiffusive mixing. The models display properties observed also in experiments: for a short time interval the behavior of the diffusion and the reaction is ordinary, in an intermediate interval the behavior is anomalous, and at long times the behavior is ordinary again.

Keywords

continuous-time random walk; subdiffusion; fractional derivative; anomalous kinetics; multistate reaction-diffusion system

AMS subject classifications

35K57; 60J60; 92C45

1. Introduction

Quantitative models of reaction-diffusion systems are important tools to theoretically and computationally study the dynamics of intracellular control systems. Macromolecules such as proteins, mRNA and DNA interact in regulatory pathways in which each chemical reaction occurs in a certain part of the cell. Molecules are transported via diffusion or active transport to arrive at the subcellular location needed to fulfill their function. As an example, in many gene regulatory pathways, proteins called transcription factors will diffuse and search for the correct binding site on DNA, where they modulate the translation of DNA into mRNA, which in turn will be translated into proteins. Apart from the spatial dynamics, realistic models need to account for large fluctuations in the copy numbers of the species due to the small reaction volume and thus the small number of molecules of key species such as transcription factors. To that end, spatial stochastic models based on a Markov

process formalism are popular due to their high level of biological realism compared to macroscopic partial differential equations (PDE), with only a moderate increase in computational complexity and cost. Such mesoscopic models, based on the so called Reaction-Diffusion Master Equation (RDME), have recently been used to address different biological phenomena such as regulation of cell division in *E. coli* [11], yeast polarization [31] and genetic oscillators [50].

A fundamental assumption in the RDME models is that molecules are point particles. Thus, the model does not account for molecular volume exclusion, something that can lead to anomalous diffusion in the crowded compartments of living cells. Especially on 2D membranes, crowding and anomalous diffusion behavior can be expected to have an impact on the reaction kinetics. For diffusion limited reactions, subdiffusion often results in a slower decay [54]. A reversible ligand binding bimolecular reaction on a 2D membrane is studied in [46] where anomalous diffusion is simulated with a continuous-time random walk (CTRW). The steady state distribution of the bound complex depends critically on the anomalous diffusion and its parameters. An irreversible bimolecular reaction is simulated in [1] with ordinary diffusion and a modified non-Fickian diffusion which is anomalous for intermediate time but tends to ordinary diffusion in the long term. The distribution of the reactant is sensitive to the type of diffusion. The conclusion in [40] is also that subdiffusion changes the reaction rate in a bimolecular reaction.

To capture effects of subdiffusion due to molecular crowding in stochastic reaction diffusion simulations, detailed Brownian Dynamics (BD) models based on a hard-sphere assumption can be used instead of the mesoscopic RDME model, since they account for the volume exclusion of molecules. However, this comes at the price of a very large increase in computational cost, making simulations on the timescales of interest in systems biology (minutes to hours) challenging. Thus there is a need to investigate less computationally demanding approximations of mesoscopic subdiffusion. A promising approach for mesoscopic anomalous diffusion simulation was suggested recently by Mommer and Lebiedz [38], in which a stochastic CTRW model [39] is approximated by an internal states model where all transitions between states have exponentially distributed waiting times. Hence, the subdiffusive process is simulated as a coupled reaction-diffusion system with ordinary diffusion, making it easily implemented in software frameworks based on the RDME [8, 18, 22].

Starting from the viewpoint that the mesoscopic model arises as an approximation of molecular crowding on the microscopic level, the internal states model can be viewed as a mathematical means to arrive at an approximate, faster simulation method. On a more general level, such internal states models arise also from the need to model for example conformational changes of macromolecules. Many proteins exist in a number of different states due to e.g. ligand binding, methylation, and conformational changes [4, 9]. In practical modeling, if each state is to be represented as a separate chemical species, an exponential growth in model complexity due to a combinatorial explosion in the number of states may be the consequence. To handle this from a practical point of view, special rule-based modeling languages have been developed, such as BioNetGen Language [3] and PySB [33]. This combinatorial explosion in states motivates the development of computational methods to

simulate models with these types of molecules more efficiently [49]. In this case, we start with an internal states model naturally arising from the biological model, and are then interested in how this model can be approximated on a phenomenological, macroscopic level as a fractional PDE (FPDE).

Molecules transported by subdiffusion move slower than with ordinary diffusion [36] which could be an effect of crowding in a biological cell. The governing equation for subdiffusion is a FPDE with a fractional time derivative and the Laplacian as the diffusive space operator. Chemical reactions can also be included in this framework. Three different models for monomolecular reactions with subdiffusion are derived and compared with analytical solutions in [21]. In one of the models where the fractional derivative acts only on the diffusion, the concentration of the species can become negative, making it less suitable. In the preferred model, where a special fractional derivative is derived for the diffusion, the equation for the homogeneous solution is recovered without a fractional derivative. The model where the fractional derivative is applied to both the diffusion and the reaction is used in [53] for a bimolecular reaction. A model with internal states is derived in [43] for the propagation of a reaction front in an inhomogeneous medium. The particles move by diffusion and react with each other at the front. Macroscopic equations are obtained after summation over the internal states. Analytical results show that the speed of the front depends on the type of reaction and the particle distribution between the internal states. That same model is suggested in [44] to explain the results in [46].

In this paper, we develop theory to extend the mesoscopic anomalous diffusion internal states model [38] to account also for chemical reactions, making it possible to model general reaction-diffusion processes. In particular, we develop theory for the connection between the model framework that thus emerges and existing models of anomalous reaction-diffusion processes on the macroscopic, FPDE level. As we will see, the proposed reactive internal states model is quite general and can, depending on the involved parameters, result in different mean-field equations. Some of these mesoscopic equations have a simple interpretation at the macroscopic level as a FPDE but in general this is not possible. In numerical simulations, the reaction-diffusion systems have the same behavior as observed in many experiments: in a short time interval after start we see ordinary behavior, then there is an anomalous phase, and finally the behavior is ordinary again but with different diffusion and reaction coefficients. These conclusions are supported theoretically in [23, 25, 30, 41]. The reaction-diffusion equations encompass many of the known models of subdiffusive reaction systems, making it promising as a general modeling framework.

The rest of the paper is organized as follows. In Section 2, we review some basic properties of stochastic models of diffusion and how they give rise to a phenomenological, macroscopic FPDE in the thermodynamic limit. Here, we will also see how the addition of chemical reactions on the macroscopic level can lead to two different, possible FPDE models. We introduce an internal states model of reaction-subdiffusion systems in Section 3 and analyze its mean field properties. In Section 4, we relate the models in Sections 2 and 3 to each other for linear and non-linear chemical reactions, and in Setion 5, numerical experiments are presented. Finally, the paper is concluded in Section 6.

2. Fractional partial differential equations as limits of continuous-time random walks

In this section, we recall some well-known facts about Brownian and, in particular, subdiffusive random movements. When approached in the proper macroscopic limit, FPDEs emerge as a convenient mathematical model for subdiffusion. Terms are added to the FPDEs to model chemical reactions.

The CTRW model was introduced by Montroll and Weiss for hopping transport on a disordered lattice [39]. In this model in continuous space, the particle is assumed to traverse the space by a series of jumps. The displacement and the waiting time to perform the next jump are drawn from a given probability density function (PDF) $\Psi(\boldsymbol{x}, t)$. We assume that the jump length PDF $\lambda(\boldsymbol{x})$ and waiting time PDF $\psi(t)$ are independent random variables. Consequently, $\Psi(\boldsymbol{x}, t)$ is written

$$\Psi(\boldsymbol{x}, t) = \psi(t)\,\lambda(\boldsymbol{x}). \quad (2.1)$$

Different diffusion processes can be categorized by the expected waiting time

$$\tau^* = \int_0^\infty t\psi(t)\,dt, \quad (2.2)$$

and the jump length variance

$$\sum{}^2 = \int_{\mathbb{R}^d} \|\boldsymbol{x}\|_2^2 \lambda(\boldsymbol{x})\,d\boldsymbol{x}, \quad (2.3)$$

where d is the dimension of the embedding space. If both Σ^2 and τ^* are finite, the long-time limit corresponds to Brownian motion. A diverging τ^* with finite Σ^2 gives rise to subdiffusion. On the contrary, a diverging Σ^2 with a finite τ^* induces superdiffusion [23, 36], which is beyond the scope of this article.

2.1. Brownian motion

We consider a Gaussian jump length PDF

$$\lambda(\boldsymbol{x}) = \frac{1}{(4\pi\sigma^2)^{d/2}} e^{-\|\boldsymbol{x}\|_2^2/(4\sigma^2)} \quad (2.4)$$

and a Poissonian waiting time PDF

$$\psi(t) = \frac{1}{\tau} e^{-t/\tau}. \quad (2.5)$$

Equations (2.2)–(2.3) lead to $\Sigma^2 = 2\sigma^2 < \infty$ and $\tau^* = \tau < \infty$. Since Σ^2 and τ^* are finite, the long-time limit thus corresponds to Brownian motion. At the macroscopic scale, we recover the classical diffusion equation [23, 36] for the concentration U of the chemical species A

$$\frac{\partial U}{\partial t} = D\Delta U, \quad (2.6)$$

with

$$D = \frac{\sigma^2}{\tau} = \frac{\sum^2}{2\tau} \quad (2.7)$$

The linear time dependence of the mean squared displacement

$$\left\langle \|\boldsymbol{x}\|_2^2(t) \right\rangle = 2dDt \quad (2.8)$$

is characteristic of Brownian motion.

2.2. Subdiffusion

We consider now instead a Gaussian jump length PDF (2.4) and a waiting time PDF [28, 35]

$$\psi(t) = \frac{t^{\alpha-1}}{\tau^\alpha} E_{\alpha,\alpha}\left(-\left(\frac{t}{\tau}\right)^\alpha\right), 0<\alpha<1, \quad (2.9)$$

where

$$E_{\alpha,\alpha}\left(-\left(\frac{t}{\tau}\right)^\alpha\right) = \sum_{k=0}^{\infty} \frac{(-(t/\tau)^\alpha)^k}{\Gamma(\alpha k+\alpha)} \quad (2.10)$$

is the generalized Mittag-Leffler function. The Mittag-Leffler waiting time PDF has been observed experimentally, from polymer rheology [16], over ligand rebinding to proteins [15] and protein conformation dynamics [52], to financial market time series [34]. Equations (2.2)–(2.3) lead to $\Sigma^2 = 2\,\sigma^2 < \infty$ and $\tau^* = \infty$, which give rise to subdiffusion. At the macroscopic scale, we obtain the FPDE [23, 36]

$$\frac{\partial^\alpha U}{\partial t^\alpha} = K_\alpha \Delta U, \quad (2.11)$$

with

$$K_\alpha = \frac{\sigma^2}{\tau^\alpha} = \frac{\sum^2}{2\tau^\alpha}. \quad (2.12)$$

At the boundary $\partial\Omega$ of the domain Ω, the molecules are reflected back implying homogeneous Neumann boundary conditions at $\partial\Omega$. The operator $\frac{\partial^\alpha}{\partial t^\alpha}$ involved in (2.11) is a Caputo fractional derivative in time of order α, generalizing the usual derivative. It is defined as [5, 37]

$$\frac{\partial^\alpha U}{\partial t^\alpha} = \int_0^t \frac{(t-\tau)^{-\alpha}}{\Gamma(1-\alpha)} \frac{dU}{dt}(\tau)\, d\tau. \quad (2.13)$$

The mean squared displacement is given by the power law

$$\langle \|\boldsymbol{x}\|_2^2(t) \rangle = \frac{2dK_\alpha}{\Gamma(1+\alpha)} t^\alpha. \quad (2.14)$$

In the one dimensional (1D) case ($d = 1$) in free space, the Green's function of the FPDE (2.11) is [36]

$$U(x,t) = \frac{1}{\sqrt{4\pi K_\alpha t^\alpha}} H_{1,2}^{2,0}\left[\frac{x^2}{4K_\alpha t^\alpha} \middle| \begin{matrix} (1-\frac{\alpha}{2}, \alpha) \\ (0,1) \end{matrix} \quad \left(\tfrac{1}{2}, 1\right) \right], \quad (2.15)$$

where the Fox function $H_{1,2}^{2,0}$ is defined in Appendix A. In the particular case $\alpha = 1/2$, the Green's function (2.15) can be rewritten

$$U(x,t) = \frac{1}{\sqrt{8\pi^3 K_{1/2} t^{1/2}}} G_{0,3}^{3,0}\left[\left(\frac{x^2}{16 K_{1/2} t^{1/2}} \right)^2 \middle| \left(0, \frac{1}{4}, \frac{1}{2}\right) \right], \quad (2.16)$$

where the Meijer-G function $G_{0,3}^{3,0}$ is also defined in Appendix A. The Green's function (2.16) will be used in numerical experiments in Section 5 as a reference solution.

2.3. Adding chemical reactions

In the following we discuss how chemical reactions can be added to the macroscopic subdiffusion model (2.11) for the cases of annihilation, reversible isomerization, and reversible bimolecular reactions. As we will see, in the first two cases two different FPDE models are possible, while only one of them turns out to be well defined for bimolecular association.

2.3.1. Annihilation—We first consider one species A and the annihilation process $A \xrightarrow{k_*} \varnothing$. Two different FPDEs can be used to model an annihilation process. If a constant proportion of walkers are removed instantaneously at the start of each step then the long-time asymptotic limit yields a fractional reaction-diffusion equation with a fractional order temporal derivative operating both on the standard diffusion term and on the linear reaction kinetics term [21, 24, 42]:

$$\frac{\partial U}{\partial t} = \frac{\partial^{1-\alpha}}{\partial t^{1-\alpha}} \left(K_\alpha \Delta U - k_* U \right). \quad (2.17)$$

In what follows, (2.17) is referred to as *model I*. The total amount $\bar{U}$ of A in a bounded domain Ω with boundary ∂Ω is defined as

$$\overline{U} = \int_\Omega U(\boldsymbol{x}, t) d\Omega. \quad (2.18)$$

The equation (2.17) is integrated over Ω

$$\frac{d\overline{U}}{dt} = \frac{\partial^{1-\alpha}}{\partial t^{1-\alpha}} \left(K_\alpha \int_\Omega \Delta U d\Omega - k_* \overline{U} \right). \quad (2.19)$$

Since

$$\int_\Omega \Delta U d\Omega = \int_{\partial\Omega} \boldsymbol{n} \cdot \nabla U dS = 0 \quad (2.20)$$

for Neumann conditions at ∂Ω with normal $\boldsymbol{n}$, $\bar{U}$ satisfies the fractional ordinary differential equation (ODE)

$$\frac{d^\alpha \overline{U}}{dt^\alpha} = -k_* \overline{U}. \quad (2.21)$$

Consequently, the total amount of A is also affected by the subdiffusion. This behavior is called *anomalous kinetics*. In the 1D case in free space, the Green's function of (2.17) is [21]

$$U(x,t) = \frac{1}{\sqrt{4\pi K_\alpha t^\alpha}} \sum_{j=0}^{\infty} \frac{(-k_* t^\alpha)^j}{j!} H_{1,2}^{2,0} \left[\frac{x^2}{4K_\alpha t^\alpha} \middle| \begin{matrix} (1 - \frac{\alpha}{2} + \alpha j, \alpha) \\ (0,1) \end{matrix} \quad \begin{matrix} \\ \left(\frac{1}{2} + j, 1\right) \end{matrix} \right]. \quad (2.22)$$

In the particular case of α = 1/2, (2.22) can be rewritten as

$$U(x,t)=\frac{1}{\sqrt{8\pi^3 K_{1/2}t^{1/2}}}\sum_{j=0}^{\infty}\frac{\left(-2k_*t^{1/2}\right)^j}{j!}G_{0,3}^{3,0}\left[\left(\frac{x^2}{16K_{1/2}t^{1/2}}\right)^2\Big|\left(0,\frac{1}{4},\frac{j}{2},\frac{1}{2}\right)\right]. \quad (2.23)$$

If instead the walkers are removed at a constant per capita rate during the waiting time between steps then the long time asymptotic limit has a standard linear reaction kinetics term but a fractional order temporal derivative operating on a nonstandard diffusion term [21, 32, 45, 51]:

$$\frac{\partial U}{\partial t}=K_\alpha e^{-k_*t}\frac{\partial^{1-\alpha}}{\partial t^{1-\alpha}}\left(e^{k_*t}\Delta U\right)-k_*U. \quad (2.24)$$

This case is referred to as *model II* in what follows. Integrating (2.24) and using (2.20) leads to

$$\frac{\partial \overline{U}}{\partial t}=K_\alpha e^{-k_*t}\frac{\partial^{1-\alpha}}{\partial t^{1-\alpha}}\left(e^{k_*t}\int_\Omega \Delta U d\Omega\right)-k_*\overline{U}=-k_*\overline{U}. \quad (2.25)$$

Ordinary kinetics is recovered: the total amount of A is not affected by the subdiffusion. The change of variables $\overline{U}=e^{k_*t}U$ in (2.24) leads to the FPDE (2.11). In the one dimensional case, the Green's solution of (2.24) is then [21, 36]

$$U(x,t)=\frac{e^{-k_*t}}{\sqrt{4\pi K_\alpha t^\alpha}}H_{1,2}^{2,0}\left[\frac{x^2}{4K_\alpha t^\alpha}\Big|\begin{matrix}(1-\frac{\alpha}{2},\alpha)\\(0,1)\end{matrix}\quad\left(\frac{1}{2},1\right)\right]. \quad (2.26)$$

2.3.2. Monomolecular reactions—Let two species A and B undergo the monomolecular reversible isomerization reaction $A\underset{\ell_*}{\overset{k_*}{\rightleftharpoons}}B$. We assume that the jump length variance and the time scale involved in (2.12) are the same for each species: $\sum_A^2=\sum_B^2$ and $\tau_A=\tau_B=\tau$. Consequently, the diffusion coefficients are also identical $K_{Aa}=K_{Ba}=K_a$. The concentrations of A and B are U and V, respectively. As in the case of annihilation, two different FPDEs can be used to model this reaction. Model I is here written

$$\frac{\partial \boldsymbol{U}}{\partial t}=K_\alpha\frac{\partial^{1-\alpha}}{\partial t^{1-\alpha}}\left(\Delta \boldsymbol{U}-\boldsymbol{R}\boldsymbol{U}\right), \quad (2.27)$$

with $U=(U\ V)^T$ and $\boldsymbol{R}=\begin{pmatrix}k_* & -\ell_*\\ -k_* & \ell_*\end{pmatrix}$ The reaction matrix $\boldsymbol{R}$ is diagonalizable, $\boldsymbol{R}=\boldsymbol{P}\,\boldsymbol{\Lambda}_r\,\boldsymbol{P}^{-1}$, with

$$\boldsymbol{P}=\begin{pmatrix} 1 & \ell_* \\ -1 & k_* \end{pmatrix}, \boldsymbol{\Lambda}_r=\begin{pmatrix} k_*+\ell_* & 0 \\ 0 & 0 \end{pmatrix}. \quad (2.28)$$

\By setting $\tilde{\boldsymbol{U}} = \boldsymbol{P}^{-1}\,\mathbf{U}$, the governing system of evolution equations decouples to

$$\frac{\partial \tilde{\boldsymbol{U}}}{\partial t}=K_\alpha \frac{\partial^{1-\alpha}}{\partial t^{1-\alpha}}\left(\Delta\tilde{\boldsymbol{U}}-\boldsymbol{\Lambda}_r\tilde{\boldsymbol{U}}\right). \quad (2.29)$$

In the 1D case without boundaries, the Green's function of the FPDE (2.29) can be computed using (2.15) and (2.22).

Model II is written

$$\frac{\partial \boldsymbol{U}}{\partial t}=K_\alpha e^{-\boldsymbol{R}t}\frac{\partial^{1-\alpha}}{\partial t^{1-\alpha}}\left(e^{\boldsymbol{R}t}\Delta\boldsymbol{U}\right)-\boldsymbol{R}\boldsymbol{U}, \quad (2.30)$$

The change of variables $\tilde{\boldsymbol{U}}=e^{\boldsymbol{R}t}\boldsymbol{U}$ in (2.30) leads to the FPDE (2.11). The Green's function of the FPDE (2.30) in 1D can be computed using (2.26).

2.3.3. Bimolecular reactions—Finally, we consider three species A, B and C and the reversible bimolecular reaction $A+B\underset{\ell_*}{\overset{k_*}{\rightleftharpoons}}C$. As previously, we assume that the jump length variance and the time scale involved in (2.12) are the same for all species, which implies that the diffusion coefficients are also identical. The concentrations of A, B and C are U, V and W, respectively. In the bimolecular case, due to the nonlinearity, only model I is defined. It is written

$$\begin{cases} \frac{\partial U}{\partial t}=K_\alpha\frac{\partial^{1-\alpha}}{\partial t^{1-\alpha}}\left(\Delta U-k_*UV+\ell_*W\right), \\ \frac{\partial V}{\partial t}=K_\alpha\frac{\partial^{1-\alpha}}{\partial t^{1-\alpha}}\left(\Delta V-k_*UV+\ell_*W\right), \\ \frac{\partial W}{\partial t}=K_\alpha\frac{\partial^{1-\alpha}}{\partial t^{1-\alpha}}\left(\Delta W+k_*UV-\ell_*W\right). \end{cases} \quad (2.31)$$

No analytical solution is available in this case. Nevertheless, the quantity $U-V$ satisfies the FPDE (2.11). Consequently, the analytical solution of $U-V$ is given by (2.15).

3. The internal states model

In this section, we introduce an internal states model of subdiffusion on the mesoscale. The molecules jump on a lattice and can react with each other when they are in the same lattice cell. Diffusion is here modeled by discrete jumps with a waiting time PDF $\psi(t)$ and a jump length depending on the nearest neighbors in the lattice.

3.1. Mesoscopic diffusion and reactions

In the stochastic mesoscopic model, the state of the system at time t is given by the number of molecules of each one of the N species in the state vector $\mathbf{y}(t) \in \mathbb{Z}_+^N$. The domain is partitioned into non-overlapping voxels or compartments $\mathscr{V}_i$, $i = 1, \ldots, M$, with a mesh or a lattice. Each voxel has a vertex at x_i in the center. The component y_{jk} of $\mathbf{y}_k$ is the number of molecules of species j in $\mathscr{V}_k$. The states are changed randomly at discrete time points t_ℓ depending on chemical reactions or a jump to a neighboring voxel due to diffusion. Between t_ℓ and $t_{\ell+1}$, $\mathbf{y}$ is constant. The PDF is $p(\mathbf{y}, t)$ for the system to be in state $\mathbf{y}$ at time t, and satisfies a master equation [10, 26], commonly referred to as the Reaction-Diffusion Master Equation (RDME) in the context of chemical kinetics.

The jump coefficient λ_{ji} for a diffusive jump of a molecule A from $\mathscr{V}_j$ to $\mathscr{V}_i$ is determined from the coefficients of a discretized diffusion equation in [10]. The rate for a jump is $\lambda_{ji} y_j$ where y_j is the copy number of A in $\mathscr{V}_j$. After the diffusive jump, y_j and y_i are updated: $y_j := y_j - 1$, $y_i := y_i + 1$.

A bimolecular reaction between the molecular species A and B produces a C molecule in a voxel in

$$A + B \xrightarrow{\kappa} C. \quad (3.1)$$

The propensity of the reaction is κ times the copy numbers y and z of A and B. If the reaction takes place at t_ℓ then the state before the reaction $\mathbf{y}\left(t_\ell^-\right)$ in the voxel is changed to $\mathbf{y}\left(t_\ell^+\right) = \mathbf{y}\left(t_\ell^-\right) + \boldsymbol{\nu}_r$ immediately after the reaction r, where $\boldsymbol{\nu}_r$ is the stoichiometric vector associated with the reaction. In (3.1), $y := y - 1$, $z := z - 1$, and the copy number of C increases by one.

A realization of the chemical system is generated by the stochastic simulation algorithm (SSA) [13] in a Monte Carlo method. In the limit of large copy numbers, the mean values of the concentrations of the species converge to the solution of the reaction rate equations [29]. These equations are stated in Section 3.3.

In the next section, a master equation is derived for the PDF of a system with internal states. Internal states of the species are introduced in [38] to model subdiffusion. We will extend their model to include reactions between the species.

3.2. A generalized master equation

As a generalization of the classical chemical master equation (CME), we let a chemical species A have a number N of internal states A_l, $l = 1, \ldots, N$. The state A_l can model a conformational state that can be difficult to observe and that is more or less hidden from a practical point of view as in a hidden Markov model. On the molecular level, the hidden states can model different things, for example, they can represent different geometrical

configurations of the molecule or the macromolecule can have different small molecules attached to it at different locations [4, 9].

We now consider a general event q which could be a diffusive jump, a change of internal states or a reaction. Assume that the molecule in the state j has a PDF for the waiting time with density $\psi_{qj}(t)$ for the event q and that the molecule, due to the event, then changes state to i with probability π_{qij} such that $\sum_i \pi_{qij}=1$. Although formally $\psi_{qj}(t)$ here is slightly different from the one in Section 2, the notation is retained since the observed effects are the same. Usually, the waiting time is assumed to be exponentially distributed and dependent on reaction rates and diffusion propensities.

The Laplace transform of a function f(t) is denoted by $\tilde{f}(s)$. An auxiliary function $\phi_{qj}(t)$ is defined by its Laplace transform involving the Laplace transform of the waiting time PDF $\tilde{\psi}_{qj}(s)$

$$\tilde{\phi}_{qj}(s)=s\tilde{\psi}_{qj}(s)/(1-\tilde{\psi}_{qj}(s)) \quad (3.2)$$

Gillespie shows in [14] (see also [19, 27]) that there is a generalized master equation for the PDF p_i of state i

$$\frac{\partial p_i(t)}{\partial t}=\sum_q \int_0^t \sum_j (\pi_{qij}\phi_{qj}(t-t')p_j(t') - \pi_{qji}\phi_{qi}(t-t')p_i(t'))dt' \quad (3.3)$$

If $\psi_{qi}(t) = a_{qi}\exp(-a_{qi}t)$, then $\phi_{qi}(t) = a_{qi}\,\delta(t)$ where $\delta(t)$ is the Dirac delta and a_{qi} is the reaction propensity. Then we obtain the usual master equation

$$\frac{\partial p_i(t)}{\partial t}=\sum_q\sum_j (\pi_{qij}a_{qj}p_j(t) - \pi_{qji}a_{qi}p_i(t))=\sum_q\sum_j (\pi_{qij}a_{qj}p_j(t)) - a_{qi}p_i(t). \quad (3.4)$$

Let state i be $\mathbf{y}$ and let state j be $\mathbf{y}-\boldsymbol{\nu}_q$ in (3.4) and identify $a_q(\mathbf{y}-\boldsymbol{\nu}_q)$ with $\pi_{qij}\,a_{qj}$ and a_{qi} with $a_q(\mathbf{y})$ for event q. Let Q be the total number of events. If the waiting times are exponentially distributed then we recover the usual CME [26]

$$\frac{\partial p(\mathbf{y},t)}{\partial t}=\sum_{q=1}^{Q}(a_q(\mathbf{y}-\boldsymbol{\nu}_q)p(\mathbf{y}-\boldsymbol{\nu}_q,t) - a_q(\mathbf{y})p(\mathbf{y},t)). \quad (3.5)$$

We consider six different elementary events listed in Table 3.1. The coefficients in (3.4) and waiting times in (3.2) defining the events are also found in Table 3.1. The copy numbers of the species A_j and B_i are y_j and z_i, respectively. The total rates away from the state in the table to all other states that can be reached are

$$\sum_i \mu_i = 1, \lambda_k = \sum_\ell \lambda_{\ell k}, \kappa_j = \sum_i \kappa_{ji}, \kappa_{ij} = \sum_k \kappa_{ijk}$$

ensuring that $\sum_i \pi_{ij} = 1$. The waiting time distribution in the state is $\psi_j(t) = a_j \exp(-a_j t)$ when one molecule is transformed in Table 3.1. The time scale τ_j of the transformations depends on the internal state j of A. We will find that if $\tau_i \neq \tau_j$ when $i \neq j$ then the annihilation, diffusion, reaction, or production is anomalous at the macroscopic level. If $\tau_i = \tau$ then the transformation between the states is the ordinary one with the same waiting time for all states.

The scale τ_{ij} of the bimolecular reaction depends on the states of A and B. By splitting the reaction rate into $\theta \kappa_{ijk}/\tau_i + (1-0)\,\kappa_{ijk}/\tau_j$ with $0 \leq \theta \leq 1$, the time constant is $\tau_{ij} = 1/(\theta \tau_i^{-1} + (1-\theta)\tau_j^{-1})$. This τ_{ij} is in agreement with the time scale obtained from [6]. Let D_{Ai} and D_{Bi} be the diffusion coefficients of species A and B in state i, k_b the microscopic reaction rate, and ρ_r the reaction radius. Then the reaction rate κ_{ijk} in [6] follows from Smoluchowski's rate law and is a function of D_{Ai} and D_{Bj}

$$\kappa_{ijk} = \frac{k_b 4\pi \left(D_{Ai} + D_{Bj}\right) \rho_r}{k_b + 4\pi \left(D_{Ai} + D_{Bj}\right) \rho_r}. \quad (3.6)$$

Let the diffusion coefficients of species A and B depend on the internal state such that $D_{Ai} = \sigma_A^2/\tau_i$ and $D_{Bj} = \sigma_B^2/\tau_j$ (2.7). Then with $\theta = \sigma_A^2/\left(\sigma_A^2 + \sigma_B^2\right)$ and for diffusion limited systems with a large k_b compared to $D_{Ai} + D_{Bj}$, κ_{ijk} is approximated by

$$\kappa_{ijk} \approx 4\pi \left(\sigma_A^2 + \sigma_B^2\right) \left(\frac{\theta}{\tau_i} + \frac{1-\theta}{\tau_j}\right). \quad (3.7)$$

When k_b is small then the influence of the diffusion disappears in (3.6) and $\kappa_{ijk} \approx k_b$ without dependence on the states i and j.

With the master equation (3.4) or (3.5), we can derive reaction rate equations approximately satisfied by the mean values as in [26, 38].

3.3. Mean-field properties of the internal states model

The mean values of the concentrations of the species approximately satisfy a system of ODEs often denoted the reaction rate equations. These equations are derived from the PDF in the master equation (3.4) or (3.5), see [26]. When the reactions are such that all propensities are linear in the chemical system, see Table 3.1, then the solutions to the equations are the exact mean values. They are approximations if there is a bimolecular reaction in the chemical system.

3.3.1. Diffusion—Let us first examine a system with one molecular species and N internal states. This is the problem investigated in [38]. We allow changes of internal state and diffusion between two voxels but without chemical reactions. The mean values of the concentrations of the N states $\mathbf{u}_i(t) \in \mathbb{R}^N$ in voxel i are the solution of

$$\frac{\partial \mathbf{u}_i}{\partial t} = \sigma^2 \left(\sum_{j=1}^{n_i} \frac{\lambda_{ij}}{\tau_i} \mathbf{u}_j - \frac{\lambda_i}{\tau_i} \mathbf{u}_i \right) + A\mathbf{u}_i = \frac{\sigma^2}{\tau_i} \left(\sum_{j=1}^{n_i} \lambda_{ij} \mathbf{u}_j - \lambda_i \mathbf{u}_i \right) + A\mathbf{u}_i. \quad (3.8)$$

The number of voxels directly connected to $\mathcal{V}_i$ is n_i. Consequently, a diffusive jump between $\mathcal{V}_j$ $i \neq j$, and $\mathcal{V}_i$ is possible. The elements of $\boldsymbol{A}$ follow from Table 3.1 and are $A_{ij} = \mu_i / \tau_j$, and $A_{ii} = (\mu_i - 1)/\tau_i$. Let $\boldsymbol{T}$ be a diagonal matrix with $T_{ii} = 1/\tau_i$, $\boldsymbol{\mu}$ a vector with non-negative components μ_i such that $\mathbf{e}^T \boldsymbol{\mu} = 1$ and $\mathbf{e}$ a vector with $e_i = 1$ for all i. Then $\boldsymbol{A}$ in (3.8) can be written

$$\boldsymbol{A} = \left(\boldsymbol{\mu} \mathbf{e}^T - \boldsymbol{I} \right) \boldsymbol{T}. \quad (3.9)$$

The nullspace consists of one vector $\tilde{\mathbf{u}}_\infty$ where

$$\tilde{\mathbf{u}}_\infty = \boldsymbol{T}^{-1} \boldsymbol{\mu}. \quad (3.10)$$

The left eigenvector of $\boldsymbol{A}$ corresponding to eigenvalue $\lambda_1 = 0$ is e such that

$$\mathbf{e}^T \boldsymbol{A} = 0. \quad (3.11)$$

The diffusion jump coefficients in (3.8) are derived such that the Laplacian is approximated in voxel i

$$\Delta \mathbf{u}(\boldsymbol{x}, t) \approx \sum_{j=1}^{n_i} \lambda_{ij} \mathbf{u}_j - \lambda_i \mathbf{u}_i. \quad (3.12)$$

On a Cartesian mesh with equal mesh spacing h, $\lambda_{ji} = 1/h_2$ and $\lambda_i = 2d/h2$ where d is the dimension. On an unstructured mesh, the coefficients can be derived by a finite element method as in [10]. With a continuous $\mathbf{u}(x, t)$ in space, the equation approximated by (3.8) is

$$\frac{\partial \mathbf{u}}{\partial t} = \boldsymbol{D} \Delta \mathbf{u} + \boldsymbol{A}\mathbf{u}, \quad \boldsymbol{D} = \sigma^2 \boldsymbol{T}. \quad (3.13)$$

The boundary conditions are of Neumann type at the boundary to preserve the total concentration of the species as in (2.20). The analysis is simplified in this section if we

consider the solution $\mathbf{u}(x, t)$ of (3.13) instead of the discrete solutions $\mathbf{u}_j(t)$ in the voxels in (3.8).

With positive initial data, it is easy to see that there is a unique positive steady-state solution $\tilde{\mathbf{u}}_\infty$ as $t \to \infty$. This solution is space independent. We write this in the normalized form

$$\lim_{t\to\infty} \mathbf{u}(\boldsymbol{x}, t) = \tilde{\mathbf{u}}_\infty = u\mathbf{u}_\infty, \quad (3.14)$$

where $\|\mathbf{u}_\infty\|_1 = 1$ and $u = \|\mathbf{u}(x, 0)\|_1$ by the preservation of mass. Since $\Delta\mathbf{u}_\infty = 0$ we have $\boldsymbol{A}\mathbf{u}_\infty = 0$ and $\mathbf{u}_\infty$ is given by (3.10) and (3.14).

Expand the solution of (3.13) in a cosine series in 1D

$$\mathbf{u}(x, t) = \sum_{\omega=0}^{\infty} \mathbf{u}_\omega(t) \cos(\omega x), \quad (3.15)$$

with x in $[0, 2\pi]$ and insert into (3.13). Then each mode $\mathbf{u}_\omega$ satisfies

$$\frac{\partial \mathbf{u}_\omega(t)}{\partial t} = \left(-\omega^2\sigma^2\boldsymbol{T} + \boldsymbol{A}\right)\mathbf{u}_\omega(t). \quad (3.16)$$

The solution to the equation is

$$\mathbf{u}_\omega(t) = \boldsymbol{S}\exp(\boldsymbol{\Lambda}t)\boldsymbol{S}^{-1}u_\omega(t) \quad (3.17)$$

where $\boldsymbol{S}(\omega) = (s_1, s_2, \ldots, s_N)$ is the eigenvector matrix of $-\omega^2\sigma^2\boldsymbol{T} + \boldsymbol{A}$ and the eigenvalues $\lambda_j(\omega)$ are on the diagonal of $\boldsymbol{\Lambda}$. By Gerschgorin's theorem for the eigenvalues of a matrix, the eigenvalues all satisfy $\Re\lambda_j \le 0$ for $\omega = 0$ and $\Re\lambda_j < 0$ for $\omega > 0$. Thus, as t increases all modes vanish except for one mode $\mathbf{s}_1(0) = \mathbf{u}_\infty$ at $\omega = 0$ with eigenvalue $\lambda_1 = 0$.

The concentrations of the internal states are summed at the macroscopic level. Then $U = \mathbf{e}^T\mathbf{u}$ satisfies

$$\begin{aligned}\frac{\partial U(\boldsymbol{x},t)}{\partial t} = \mathbf{e}^T\left(\sigma^2\boldsymbol{T}\Delta\mathbf{u} + A\mathbf{u}\right) &= \sigma^2\mathbf{e}^T\boldsymbol{T}\Delta\mathbf{u} = \textstyle\sum_\omega -\omega^2\sigma^2\mathbf{e}^T\boldsymbol{T}\mathbf{u}_\omega(t)\cos(\omega\boldsymbol{x}) \\ &= \overline{\gamma}(\boldsymbol{x}, t)\,\mathbf{e}^T\Delta\mathbf{u} = \overline{\gamma}(\boldsymbol{x}, t)\,\Delta u, \end{aligned} \quad (3.18)$$

where

$$\overline{\gamma}(x,t) = \sigma^2 \frac{\sum_{\omega=0}^{\infty} -\omega^2 \mathbf{e}^T \boldsymbol{T} \mathbf{u}_\omega(t) \cos(\omega x)}{\sum_{\omega=0}^{\infty} -\omega^2 \mathbf{e}^T \mathbf{u}_\omega(t) \cos(\omega x)} \tag{3.19}$$

The macroscopic U satisfies a diffusion equation with a diffusion coefficient varying in space and time. For large t, the dominant mode in the spatially non-constant part of the solution is damped by the eigenvalue $\lambda_1 = \max_{j,w} \lambda_j(\omega) < 0$ at ω_1. Then $\mathbf{u}_\omega \approx \mathbf{s}_1(\omega_1) e^{\lambda_1 t}$ and the steady-state macroscopic diffusion coefficient in (3.19) is

$$\begin{aligned} \overline{\gamma} &\approx \sigma^2 \frac{\omega_1^2 \mathbf{e}^T \boldsymbol{T} \mathbf{s}_1 \mathbf{e}^{\lambda_1 t} \cos(\omega_1 \boldsymbol{x})}{\omega_1^2 \mathbf{e}^T \mathbf{s}_1 \mathbf{e}^{\lambda_1 t} \cos(\omega_1 \boldsymbol{x})} \\ &= \sigma^2 \frac{\mathbf{e}^T \boldsymbol{T} \mathbf{s}_1}{\mathbf{e}^T \mathbf{s}_1} = \sigma^2 \frac{\sum_{i=1}^{N} s_{1i}/\tau_i}{\sum_{i=1}^{N} s_{1i}}. \end{aligned} \tag{3.20}$$

3.3.2. A reversible reaction—Consider next the simple case of a reversible isomerization,

$$A_i \underset{\lambda_{ji}}{\overset{\kappa_{ij}}{\rightleftharpoons}} B_j, \tag{3.21}$$

which is to be understood in the sense that, for example, the rate for the jth internal state of a B-molecule to transform into the ith state of an A-molecule is λ_{ji}. These are thus two monomolecular reactions with reaction rates in Table 3.1.

We assume that the variance of the jump length, the diagonal matrix $\boldsymbol{T}$ and the vector $\boldsymbol{\mu}$ are the same for all species with identical matrices $\boldsymbol{D}$ and $\boldsymbol{A}$. Taking the mean as in (3.8) we readily arrive at the coupled set of PDEs

$$\frac{\partial \mathbf{u}}{\partial t} = \boldsymbol{D} \Delta \mathbf{u} + \boldsymbol{A} \mathbf{u} - \boldsymbol{K}_1 \mathbf{u} + \boldsymbol{L}_2 \mathbf{v}, \tag{3.22}$$

$$\frac{\partial \mathbf{v}}{\partial t} = \boldsymbol{D} \Delta \mathbf{v} + \boldsymbol{A} \mathbf{v} - \boldsymbol{K}_2 \mathbf{u} + \boldsymbol{L}_1 \mathbf{v}, \tag{3.23}$$

for some matrices $\boldsymbol{K}_1$, $\boldsymbol{K}_2$, and $\boldsymbol{L}_1$, $\boldsymbol{L}_2$ whose precise form we now determine. Define positive rate matrices $\boldsymbol{K}$ and $\boldsymbol{L}$ with $K_{ij} = \kappa_{ij}$ and $L_{ij} = \lambda_{ij}$. From the prescription (3.21) we find that in (3.22)–(3.23), the ith state is affected by the reaction terms

$$(-\boldsymbol{K}_1\mathbf{u}+\boldsymbol{L}_2\mathbf{v})_i = -\sum_{j=1}^{N} k_{ij}u_i + \sum_{j=1}^{N}\lambda_{ij}v_i, \tag{3.24}$$

$$(+\boldsymbol{K}_2\mathbf{u}+\boldsymbol{L}_1\mathbf{v})_i = +\sum_{j=1}^{N} k_{ij}u_j - \sum_{j=1}^{N}\lambda_{ij}v_i. \tag{3.25}$$

Identifying terms we obtain that

$$\boldsymbol{K}_1 = \mathrm{diag}\,(\boldsymbol{K}\,\mathbf{e})\,,\quad \boldsymbol{K}_2 = \boldsymbol{K}^T, \tag{3.26}$$

$$\boldsymbol{L}_1 = \mathrm{diag}\,(\boldsymbol{L}\,\mathbf{e})\,,\quad \boldsymbol{L}_2 = \boldsymbol{L}^T, \tag{3.27}$$

where the notation diag(**f**) denotes a diagonal matrix with f_i on the diagonal.

We are interested in the stable, space independent solutions to (3.22)–(3.23). Introduce

$$\boldsymbol{B} = \begin{pmatrix} \boldsymbol{A}-\boldsymbol{K}_1 & \boldsymbol{L}_2 \\ \boldsymbol{K}_2 & \boldsymbol{A}-\boldsymbol{L}_1 \end{pmatrix}. \tag{3.28}$$

By construction and using (3.11) we have the crucial properties that

$$B_{ii} = -\sum_{\substack{k=1 \\ k\neq i}}^{M} B_{ki}, \tag{3.29}$$

$$B_{ij} \geqslant 0,\quad i \neq j. \tag{3.30}$$

with $M = 2N$. Also, by inspection $\boldsymbol{B}$ is irreducible, i.e. there is no permutation matrix $\boldsymbol{Q}$ such that

$$QBQ^{-1} = \begin{pmatrix} \boldsymbol{E} & \boldsymbol{F} \\ \mathbf{0} & \boldsymbol{G} \end{pmatrix}. \quad (3.31)$$

Taken together, $\boldsymbol{B}$ is a $-matrix$ and this provides us with certain general stability properties.

Lemma 3.1 $(-matrix\ lemma)$**:** Suppose that a real, irreducible matrix $\boldsymbol{H} \in \mathbb{R}^{M\times M}$ satisfies (3.29)–(3.31) (with $\boldsymbol{B}$ replaced by $\boldsymbol{H}$). Then the system of ODEs

$$\boldsymbol{\xi}'(t) = \boldsymbol{H}\boldsymbol{\xi}(t) \quad (3.32)$$

has a single stable equilibrium solution $\boldsymbol{\xi}_\infty$ *as* $t \to \infty$. Moreover, if initial data $\boldsymbol{\xi}(0)$ with positive mass $\mathbf{e}^T\boldsymbol{\xi}(0) > 0$ is given, then $\mathbf{e}^T\boldsymbol{\xi}(t) = \mathbf{e}^T\boldsymbol{\xi}(0) > 0$ for all $t > 0$.

This particular formulation is discussed in detail in [26, Chap. V.3] and we note that it can also be shown to follow from the Perron-Frobenius theorem. To get some further insight into the stability we present some alternative arguments as outlined in [26, Chap. V.9, p. 129].

Proof: Consider the adjoint problem

$$\boldsymbol{\eta}'(t) = \boldsymbol{H}^T\boldsymbol{\eta}(t), \quad (3.33)$$

such that

$$\boldsymbol{\eta}(0)^T\boldsymbol{\xi}(t) = \boldsymbol{\eta}(t)^T\boldsymbol{\xi}(0). \quad (3.34)$$

Using (3.29) we see that

$$\eta_i'(t) = \sum_{\substack{k=1 \\ k\neq i}}^{M} H_{ki}(\eta_k - \eta_i)(t). \quad (3.35)$$

By the irreducibility of $\boldsymbol{H}$, the largest element in $\boldsymbol{\eta}$ decreases and the smallest element increases with time such that an all-constant vector $\boldsymbol{\eta}_\infty$ emerges in the limit. With $\boldsymbol{\eta}(0) = \mathbf{e}_i$, the ith unit vector, we recover from (3.34) the unique equilibrium solution $\tilde{\boldsymbol{\xi}}_\infty$. Also, with $\boldsymbol{\eta}(0) = \mathbf{e}$ we have $\boldsymbol{\eta}(t) = \mathbf{e}$ and mass is a preserved quantity. ❑

Apply the lemma to $\boldsymbol{B}$ in (3.28) with $\boldsymbol{\xi}^T = (\mathbf{u}^T, \mathbf{v}^T)$. Then it follows that there is a steady state $(\tilde{\mathbf{u}}_\infty, \tilde{\mathbf{v}}_\infty)$ and the initial mass $\mathbf{e}^T\mathbf{u}(0) + \mathbf{e}^T\mathrm{v}(0)$ is conserved for all t.

We now turn our attention to the equivalent reaction rates as induced by the subdiffusive reactions (3.21). We write the unique equilibrium solution $\tilde{\mathbf{u}}_\infty$, $\tilde{\mathbf{v}}_\infty$ in the normalized form $\tilde{\mathbf{u}}_\infty = u\,\mathbf{u}_\infty$, $\tilde{\mathbf{v}}_\infty = v\,\mathbf{v}_\infty$, where $\|\mathbf{u}_\infty\|_1 = \|\mathbf{v}_\infty\|_1 = 1$. Using (3.26)–(3.27) we readily find in good agreement that

$$k_{eq} := \mathbf{e}^T \boldsymbol{K}_1\,\mathbf{u}_\infty = \mathbf{e}^T \boldsymbol{K}_2\,\mathbf{u}_\infty,\quad l_{eq} := \mathbf{e}^T \boldsymbol{L}_1\,\mathbf{v}_\infty = \mathbf{e}^T \boldsymbol{L}_2\,\mathbf{v}_\infty. \tag{3.36}$$

Also, to mention just one example,

$$k_{eq}\mathbf{e}^T\,\tilde{\mathbf{u}}_\infty = \mathbf{e}^T \boldsymbol{K}_1\,\tilde{\mathbf{u}}_\infty, \tag{3.37}$$

which can be understood as a kind of consistency result; at steady state the equivalent reaction rate applied to the sum of the internal states gives the same result as the sum of the individual subdiffusive rates.

To conclude, using the subdiffusion steady state solutions, which remain valid also when the coupling reactions (3.21) are ‘turned on’, we can read off the equivalent reaction rates as a function of the corresponding subdiffusive rates. Insert $\boldsymbol{u}(\boldsymbol{x}, t) = \mathrm{u}(\boldsymbol{x}, t)\,\mathbf{u}_\infty$ and $\mathbf{v}(\boldsymbol{x}, t) = v(\boldsymbol{x}, t)\,\mathbf{v}_\infty$ into (3.22) and (3.23). Then we have

$$\mathbf{u}_\infty \frac{\partial u}{\partial t} = \boldsymbol{D}\,\mathbf{u}_\infty\,\Delta u + u\,\boldsymbol{A}\,\mathbf{u}_\infty - u\,\boldsymbol{K}_1\,\mathbf{u}_\infty + v\,\boldsymbol{L}_2\,\mathbf{v}_\infty, \tag{3.38}$$

$$\mathbf{v}_\infty \frac{\partial v}{\partial t} = \boldsymbol{D}\,\mathbf{v}_\infty\,\Delta v + v\,\boldsymbol{A}\,\mathbf{v}_\infty + u\,\boldsymbol{K}_2\,\mathbf{u}_\infty + v\,\boldsymbol{L}_1\,\mathbf{v}_\infty. \tag{3.39}$$

Multiply by $\mathbf{e}^T$ and in the long-time limit we thus arrive at the familiarly looking macroscopic reaction-diffusion PDE

$$\frac{\partial u}{\partial t} = \gamma_u\,\Delta u - k_{eq}\,u + l_{eq}\,v, \tag{3.40}$$

$$\frac{\partial v}{\partial t} = \gamma_u\,\Delta v + k_{eq}\,u - l_{eq}\,v, \tag{3.41}$$

with $\gamma_u = \mathbf{e}^T \boldsymbol{D}\,\mathbf{u}_\infty$ and $\gamma_v = \mathbf{e}^T \boldsymbol{D}\,\mathbf{v}_\infty$.

3.3.3. A bimolecular reaction—We finally consider the case of a reversible dimerization,

$$A_i + B_j \underset{\lambda_{ijk}}{\overset{\kappa_{ijk}}{\rightleftharpoons}} C_k. \tag{3.42}$$

As in Section 3.3.2, the jump length variance, the diagonal matrix $\boldsymbol{T}$ and the vector $\boldsymbol{\mu}$ are the same for each species and $\boldsymbol{D}$ and $\boldsymbol{A}$ are also identical. Due to the nonlinearities it is inconvenient to write this in a matrix form as in (3.22)–(3.23). Instead, for each internal state i we have the mean-field equations,

$$\frac{\partial u_i}{\partial t} = D_i \, \Delta u_i + \sum_{j=1}^{N} A_{ij} \, u_j - \sum_{j,k=1}^{N} K_{ijk} \, u_j \, v_j + \sum_{j,k=1}^{N} L_{ijk} \, w_k, \tag{3.43}$$

$$\frac{\partial v_i}{\partial t} = D_i \, \Delta v_i + \sum_{j=1}^{N} A_{ij} \, v_j - \sum_{j,k=1}^{N} K_{jik} \, u_j \, v_i + \sum_{j,k=1}^{N} L_{jik} \, w_k, \tag{3.44}$$

$$\frac{\partial w_i}{\partial t} = D_i \, \Delta w_i + \sum_{j=1}^{N} A_{ij} \, w_j + \sum_{j,k=1}^{N} K_{jki} \, u_j \, v_k + \sum_{j,k=1}^{N} L_{jki} \, w_i, \tag{3.45}$$

where for readability we write $K_{ijk} = \kappa_{ijk}$ and $L_{ijk} = \lambda_{ijk}$. The difference $u_i - v_i$ satisfies

$$\frac{\partial (u_i - v_i)}{\partial t} = D_i \, \Delta (u_i - v_i) + \sum_{j=1}^{N} A_{ij} \, (u_i - v_i) - \sum_{j,k=1}^{N} K_{ijk} u_i v_j - K_{jik} u_j v_i. \tag{3.46}$$

If $K_{ijk} = K_{jik}$ and $L_{ijk} = L_{jik}$ in (3.46) and $u_i(\boldsymbol{x}, 0) = v_i(\boldsymbol{x}, 0)$ for all i, then it follows that $u_i(\boldsymbol{x}, t) = v_i(\boldsymbol{x}, t)$ for $t > 0$.

Assume that there is a positive steady state solution $(\tilde{\mathbf{u}}_\infty, \tilde{\mathbf{v}}_\infty, \tilde{\mathbf{w}}_\infty)$ to (3.43)–(3.45) when $t \to \infty$. Let $(\tilde{\mathbf{u}}_\infty, \tilde{\mathbf{v}}_\infty, \tilde{\mathbf{w}}_\infty) = (u \, \mathbf{u}_\infty, \, v \, \mathbf{v}_\infty, \, w \, \mathbf{w}_\infty)$ where $\| \mathbf{u}_\infty \|_1 = \| \mathbf{v}_\infty \|_1 = \| \mathbf{w}_\infty \|_1 = 1$. Small perturbations around the equilibrium solution are evolved by the Jacobian of the system. For (3.43)–(3.45), it can be written in the form

$$\boldsymbol{B} = \begin{pmatrix} \boldsymbol{A} - \boldsymbol{K}_{11} & -\boldsymbol{K}_{12} & \boldsymbol{L}_1 \\ -\boldsymbol{K}_{21} & \boldsymbol{A} - \boldsymbol{K}_{22} & \boldsymbol{L}_2 \\ \boldsymbol{K}_{31} & \boldsymbol{K}_{32} & \boldsymbol{A} - \boldsymbol{L}_3 \end{pmatrix}. \tag{3.47}$$

We identify after some tedious work

$$\boldsymbol{K}_{11}=\mathrm{diag}\ \sum_{j,k=1}^{N} K_{ijk}\, v_{\infty j},\quad \boldsymbol{K}_{22}=\mathrm{diag}\ \sum_{j,k=1}^{N} K_{jik}\, u_{\infty j},\quad \boldsymbol{L}_{3}=\mathrm{diag}\ \sum_{j,k=1}^{N} L_{jki}, \tag{3.48}$$

$$(\boldsymbol{L}_1)_{ij}=\sum_{k=1}^{N} L_{ikj},\quad (\boldsymbol{L}_2)_{ij}=\sum_{k=1}^{N} L_{kij}, \tag{3.49}$$

$$(\boldsymbol{K}_{12})_{ij}=\sum_{k=1}^{N} K_{ijk}\, u_{\infty i},\quad (\boldsymbol{K}_{21})_{ij}=\sum_{k=1}^{N} K_{jik}\, v_{\infty i}, \tag{3.50}$$

$$(\boldsymbol{K}_{32})_{ij}=\sum_{k=1}^{N} K_{kji}\, u_{\infty k},\quad (\boldsymbol{K}_{31})_{ij}=\sum_{k=1}^{N} K_{jki}\, v_{\infty k}. \tag{3.51}$$

The Jacobian B in (3.47) is not a $-matrix$**:** To understand why, note in (3.42) that the total sum of molecules is not a preserved quantity. However, if each *C*-molecule is counted twice, this new weighted sum is in fact preserved. Indeed, by inspection and after some work we find that multiplying ***B*** by a diagonal matrix with 1 on the diagonal in the first 2*N* rows and 2 in the last *N* rows we have a $-\mathrm{matrix}$. Using the $-\mathrm{matrix}$ Lemma 3.1 it therefore follows that small perturbations around an equilibrium solution are stable.

Equivalent reaction rates can be defined as follows,

$$k_{\mathrm{eq}}=\sum_{i,j,k=1}^{N} K_{ijk}\, u_{\infty i}\, v_{\infty j},\quad l_{\mathrm{eq}}=\sum_{i,j,k=1}^{N} L_{ijk}\, w_{\infty k}. \tag{3.52}$$

Insert **u**(*x*, *t*), **v**(*x*, *t*), and **w**(*x*, *t*) = *w*(*x*, t) $\mathbf{w}_\infty$ into (3.43)–(3.45) as in (3.38) and let $\gamma_w = \mathbf{e}^T \boldsymbol{D}\, \mathbf{w}_\infty$. As expected we recover the reaction-diffusion PDE for *u*, *v*, and *w*

$$\frac{\partial u}{\partial t}=\gamma_u\, \Delta u - k_{\mathrm{eq}}\, u\, v + l_{\mathrm{eq}}\, w, \tag{3.53}$$

$$\frac{\partial v}{\partial t}=\gamma_v\, \Delta v - k_{\mathrm{eq}}\, u\, v + l_{\mathrm{eq}}\, w, \tag{3.54}$$

$$\frac{\partial w}{\partial t}=\gamma_w\,\Delta w+k_{\mathrm{eq}}\,u\,v\;-\;l_{\mathrm{eq}}\,w. \tag{3.55}$$

4. The internal states approximation of the FPDE

In this section we start off with the promising observation made in [38] that non-Markovian waiting times can be arbitrarily well approximated by a set of Markovian waiting times, each associated with its own *internal state*. In turn, those states are to be visited according to a certain random walk model which again can be taken as Markovian, all in all resulting in a computationally quite attractive modeling framework for subdiffusion and reactions.

In Section 4.1, we recapitulate the basic internal states subdiffusive model and its relation to the FPDE, and in Section 4.2 we determine its asymptotic behavior for short and long times. In Section 4.3, we consider the same framework in the presence of reactions with two different mesoscopic models. In particular, we discuss the feasibility of obtaining coarse-grained macroscopic coefficients in a FPDE from observations of subdiffusive systems.

4.1. Internal states diffusion system

The asymptotic behavior of the waiting time (2.9) at large time follows the power law

$$\psi\,(t)\approx A_\alpha\frac{\tau^\alpha}{t^{1+\alpha}}, \tag{4.1}$$

with

$$A_\alpha=\frac{\sin\,(\pi\,\alpha)}{\pi}\Gamma\,(1+\alpha)\,. \tag{4.2}$$

With a change of variable in the Euler's Γ function, the diffusive representation of the totally monotone function $\frac{1}{t^{1+\alpha}}$ in (4.1) is [7, 17, 20, 48]

$$\frac{1}{t^{1+\alpha}}=\frac{1}{\Gamma\,(1+\alpha)}\int_0^\infty s^\alpha\,e^{-st}\,ds. \tag{4.3}$$

The diffusive representation of $\frac{1}{t^{1+\alpha}}$ (4.3) is approximated by using a quadrature formula in N points, with weights $\tilde{\mu}_i$ and abscissae s_i:

$$\frac{1}{t^{1+\alpha}}\simeq\sum_{i=1}^{N}\tilde{\mu}_i\,e^{-s_i\,t}, \tag{4.4}$$

leading to the *diffusive approximation* [2].

Our objective is then to approximate the function $F_{ex}(t) = \frac{1}{t^{1+\alpha}}$ by $F_{approx}(t) = \sum_{i=1}^{N} \tilde{\mu}_i \, e^{-s_i t}$ in the time interval $[t_{min}, t_{max}]$. One possibility to quantify the error of the model ε_{mod} is

$$\varepsilon_{mod} = \| \frac{F_{approx}(t)}{F_{ex}(t)} - 1 \| = \left(\frac{1}{t_{max} - t_{min}} \int_{t_{min}}^{t_{max}} \left| \frac{F_{approx}(t)}{F_{ex}(t)} - 1 \right|^2 dt \right)^{1/2}. \quad (4.5)$$

Based on the error (4.5), a nonlinear optimization is shown in [2] to be a better way to determine the parameters $\tilde{\mu}_i$ and s_i than Gaussian quadrature. Consequently, this method is used in all what follows.

Setting

$$\tau_i = 1/s_i, \quad \tau = \left(A_\alpha \sum_{i=1}^{N} \frac{\tilde{\mu}_i}{s_i} \right)^{-1/\alpha}, \quad \mu_i = \frac{\tilde{\mu}_i}{s_i} \left(\sum_{i=1}^{N} \frac{\tilde{\mu}_i}{s_i} \right)^{-1}, \quad (4.6)$$

the approximation of the waiting time (4.1) is

$$\psi(t) \approx \sum_{i=1}^{N} \mu_i \, \tau_i^{-1} \, e^{-t/\tau_i}. \quad (4.7)$$

The jump length variance Σ^2 (2.3) is then computed using (2.12).

The waiting time PDF (2.9) and its asymptotic expansion (4.1) are compared in Figure 4.1. The parameters are those used in the numerical experiments in Section 5.2 (Table 5.1, second set of parameters). Anomalous diffusion is expected in the time range of interest $[t_{min}, t_{max}]$. In this time interval, the expansion (4.1) is already accurate as illustrated in Figure 4.1.

The CTRW algorithm in Section 2 is extended to a multistate CTRW (MCTRW) algorithm in [38] for a diffusive system with internal states. One diffusive jump in the algorithm is performed as follows. Firstly, a state i is drawn with probability μ_i. Secondly, the waiting time is sampled from an exponential distribution with the PDF $\psi_i(t) = \tau_i^{-1} e^{-t/\tau_i}$. The PDF of the jump length in an internal state i is $\lambda_i(x)$ as in (2.4) with variance σ_i^2. Finally, the length of the jump is drawn with the normal distribution of λ_i.

The combined PDFs for the jump length and the waiting time of the internal states are

$$\lambda(\boldsymbol{x}) = \sum_{i=1}^{N} \mu_i \lambda_i(\boldsymbol{x}), \quad \tilde{\psi}(t) = \sum_{i=1}^{N} \mu_i \psi_i(t) = \sum_{i=1}^{N} \mu_i \tau_i^{-1} e^{-t/\tau_i}. \tag{4.8}$$

The reaction-diffusion system (3.13) in [38] is derived from the MCTRW algorithm and the approximation (4.7). In the ith internal state, the diffusion of u_i is ordinary, whereas the sum of the concentrations of the internal states at the macroscopic level $U = \mathbf{e}^T\mathbf{u}$ diffuses anomalously within the time range $[t_{min}, t_{max}]$. A collection of internal states with waiting times $\psi_I(t)$ are here approximated by one state with the waiting time $\psi(t)$ in (4.7).

4.2. Diffusive behavior of the internal states model

To mimic a subdiffusive behavior and to define a Markov process, the waiting time PDF $\psi(t)$ is approximated by a sum of N exponentials (4.7). Let us assume that $\tau_1 < \tau_2 < \cdots < \tau_N$. Equation (4.7) implies the following.

- At small times, the Taylor expansion of $\psi(t)$ is

$$\psi(t) \approx \tilde{\psi}(t) = \sum_{i=1}^{N} \mu_i \tau_i^{-1} e^{-t/\tau_i} \approx \sum_{i=1}^{N} \mu_i \tau_i^{-1} \left(1 - \frac{t}{\tau_i}\right) \underset{t\to 0^+}{\sim} 1 - \frac{t}{\tau_{eq}} \underset{t\to 0^+}{\sim} e^{-t/\tau_{eq}}, \tag{4.9}$$

  with $\tau_{eq} = \left(\sum_{i=1}^{N} \mu_i \tau_i^{-1}\right) / \left(\sum_{i=1}^{N} \mu_i \tau_i^{-2}\right)$. At small times, $\psi(t)$ is therefore equivalent to a Poisson law with parameter τ_{eq}. Hence, ordinary diffusion is expected for $t \ll \tau_1$;
- As we see in (3.18), the macroscopic U satisfies a diffusion equation with a diffusion coefficient $\overline{\gamma}(x,t)$ (3.19) varying in space and time. For large t, the long-time diffusion coefficient is given by (3.20). It does not depend on space and time. Consequently, a return to ordinary diffusion is expected.
- For $t \in [\tau_1, \tau_N]$, a subdiffusive behavior is expected with subdiffusive exponent a.

This is in agreement with observations in physical experiments [23, 25, 30, 41]. Numerical illustrations are found in Section 5.

4.3. Internal states reaction-diffusion system

In this section, the mesoscopic model with N internal states of the participating molecules in Section 3 is compared to the macroscopic FPDE models I and II in Section 2.3. The annihilation reaction, monomolecular reactions and bimolecular reactions summarized in Table 3.1 are investigated. For mesoscopic models with certain reactions, there are

corresponding FPDE models but in other cases the macroscopic level with summation over the internal states is not so easily expressed as a FPDE.

4.3.1. Annihilation process—We consider one species A with N different internal states. Each internal state can be annihilated with rate k_i

$$A_i \xrightarrow{k_i} \varnothing, \quad i=1,\cdots,N. \tag{4.10}$$

The internal states diffusion system (3.22) without **v** is then modified as follows

$$\frac{\partial \mathbf{u}}{\partial t}=\boldsymbol{D}\Delta\mathbf{u}+\boldsymbol{A}\mathbf{u}-\boldsymbol{K}_1\mathbf{u}. \tag{4.11}$$

Let $k_i = k/\tau_i$ in (4.10) as in Table 3.1. Then $\boldsymbol{K}_1 = k\,\boldsymbol{T}$ and (4.11) can be written

$$\frac{\partial \mathbf{u}}{\partial t}=\boldsymbol{T}\left(\sigma^2\Delta\mathbf{u}-k\mathbf{u}\right)+\boldsymbol{A}\mathbf{u}. \tag{4.12}$$

In model I (2.17), the fractional order temporal derivative $\frac{\partial^{1-\alpha}}{\partial t^{1-\alpha}}$ acts on both the Laplace operator and the reaction term. In the internal states diffusion system (4.11) and (4.12), the diffusion matrix is scaled by the waiting time matrix $\boldsymbol{T}$ to mimic an anomalous behavior. Scaling the reaction matrix $\boldsymbol{K}_1$ in the same way will approximate the macroscopic model I. The waiting time $\psi_i(t)$ for diffusive and reactive events is the same for all internal states. The relation between k in (4.12) and k_* in (2.17) is the same as between σ^2 and K_α in (2.12),

$$\frac{k_*}{k}=\frac{\sigma^2}{K_\alpha}=\tau^\alpha. \tag{4.13}$$

For an approximation of model II, take $\boldsymbol{K}$ and $\boldsymbol{K}_1$ to be $k\,\boldsymbol{I}$ in (3.26). This corresponds to an annihilation case in Table 3.1 with all $\tau_i = 1$. The right hand side of (4.11) is with this $\boldsymbol{K}_1$

$$\frac{\partial \mathbf{u}}{\partial t}=\sigma^2\boldsymbol{T}\Delta\mathbf{u}+\boldsymbol{A}\mathbf{u}-k\mathbf{u}. \tag{4.14}$$

The waiting time $\psi_i(t)$ for diffusive and reactive events is different for the internal states.

If $\boldsymbol{K}_1$ and $\boldsymbol{T}$ and $\boldsymbol{K}_1$ and $\boldsymbol{A}$ commute then the equation for **u** in (4.14) can be written

$$\frac{\partial \mathbf{u}}{\partial t}=\sigma^2 e^{\boldsymbol{K}_1 t}\boldsymbol{T}e^{-\boldsymbol{K}_1 t}\Delta\mathbf{u}+e^{\boldsymbol{K}_1 t}\boldsymbol{A}e^{-\boldsymbol{K}_1 t}\mathbf{u}-k\mathbf{u}. \tag{4.15}$$

This equation corresponds to model II in Section 2.3.1 at the macroscopic level. The relation between k in (4.14) and k_* in (2.24) is

$$k_*=k. \quad (4.16)$$

After a change of variables $\tilde{U}= e^{k*t}\, U$ in the model II FPDE (2.24), the FPDE (2.30) is obtained. In the same manner, introduce a change of variables $\tilde{\mathbf{u}}=e^{\boldsymbol{K}_1 t}\,\mathbf{u}$ in (4.11). Then

$$\frac{\partial\tilde{\mathbf{u}}}{\partial t}=\sigma^2\boldsymbol{T}\Delta\tilde{\mathbf{u}}+\boldsymbol{A}\tilde{\mathbf{u}}. \quad (4.17)$$

A sufficient condition for $\boldsymbol{K}_1$ to commute with $\boldsymbol{T}$ and $\boldsymbol{A}$ is that $\boldsymbol{K}_1 = k\,\boldsymbol{I}$ as is the case in (4.14). If $\boldsymbol{K}_1$ does not commute with $\boldsymbol{T}$ and $\boldsymbol{A}$, the macroscopic equation for $U= \mathbf{e}^T\mathbf{u}$ may not be as simple as (2.30).

Consider $\bar{\mathbf{u}}$, the total amount of A in the different states in Ω, defined by

$$\overline{\mathbf{u}}\,(t)=\int_\Omega \mathbf{u}\,(\boldsymbol{x},t)\,d\Omega. \quad (4.18)$$

Integrating (4.11) and using the Neumann boundary condition in (2.19) and (2.20) leads to

$$\frac{d\overline{\mathbf{u}}}{dt}=\boldsymbol{A}\overline{\mathbf{u}}-K_1\overline{\mathbf{u}}. \quad (4.19)$$

The time evolution of $\bar{\mathbf{u}}$ is then

$$\overline{\mathbf{u}}\,(t)=\mathbf{e}^{(\boldsymbol{A}-\boldsymbol{K}_1)t}\overline{\mathbf{u}}\,(0)\,. \quad (4.20)$$

By Gerschgorin's theorem for the eigenvalues of a matrix, the eigenvalues of $\boldsymbol{A}-\boldsymbol{K}_1$ are strictly in the left half plane. By (4.19), the equation for the sum over all internal states $\bar{U}= \mathbf{e}^T\bar{\mathbf{u}}$ is

$$\frac{d\overline{U}}{dt}=-\,\mathbf{e}^T\boldsymbol{K}_1\overline{\mathbf{u}}=-\,k'\,(t)\,\overline{U}, \quad (4.21)$$

with

$$k'\,(t)=\frac{\mathbf{e}^T K_1\overline{\mathbf{u}}}{\mathbf{e}^T\overline{\mathbf{u}}}=\frac{\mathbf{e}^T K_1 e^{(\boldsymbol{A}-\boldsymbol{K}_1)t}\overline{\mathbf{u}}\,(0)}{\mathbf{e}^T e^{(\boldsymbol{A}-\boldsymbol{K}_1)t}\overline{\mathbf{u}}\,(0)} \quad (4.22)$$

In model **I** with $\boldsymbol{K}_1 = k\boldsymbol{T}$, k' varies in time depending on $\bar{\mathbf{u}}$, and the kinetics is then anomalous. Let λ_1 be the eigenvalue of $\boldsymbol{A} - \boldsymbol{K}_1$ with maximum real part and $\mathbf{s}_1$ the corresponding eigenvector. Then for large t

$$k'(t) \approx \frac{\mathbf{e}^T \boldsymbol{K}_1 \mathbf{s}_1 e^{\lambda_1 t}}{\mathbf{e}^T \mathbf{s}_1 e^{\lambda_1 t}} = k \frac{\sum_i s_{1i}/\tau_i}{\sum_i s_{1i}}, \tag{4.23}$$

cf. (3.20). On the contrary, in model **II** $k' = k$ does not depend on time, and the kinetics is then ordinary. This conclusion agrees with the comments in Section 2.3.1.

4.3.2. Monomolecular reactions—We study two species A and B with N different internal states and the reversible reactions in (3.21). The internal states diffusion system is found in (3.22) and (3.23). The aim of this section is to choose the reaction matrices $\boldsymbol{K}$ and $\boldsymbol{L}$ in (3.26) and (3.27) to mimic either model I (2.27) or model II (2.30) and to discuss other alternatives.

The reaction rates are first chosen to be scaled by the waiting time matrix and one state i is transformed to the same state i in

$$A_i \underset{\ell/\tau_i}{\overset{k/\tau_i}{\rightleftharpoons}} B_i,\ i = 1, \ldots, N. \tag{4.24}$$

Then $K_{ii} = k/\tau_i$ and $L_{ii} = \ell/\tau_i$, cf. Table 3.1. With $\boldsymbol{K} = k\boldsymbol{T}$ and $\boldsymbol{L} = \ell\boldsymbol{T}$ in (3.22) and (3.23) we have

$$\begin{aligned} \frac{\partial \mathbf{u}}{\partial t} &= \boldsymbol{T}(\sigma^2 \Delta \mathbf{u} - k\mathbf{u} + \ell \mathbf{v}) + \boldsymbol{A}\,\mathbf{u}, \\ \frac{\partial \mathbf{v}}{\partial t} &= \boldsymbol{T}(\sigma^2 \Delta \mathbf{v} - k\mathbf{u} + \ell \mathbf{v}) + \boldsymbol{A}\,\mathbf{v}. \end{aligned} \tag{4.25}$$

The diffusion and the reactions have the same waiting time as in model I in (2.27).

The steady state of model I in (4.25) has an analytical solution. Let $\mathbf{u}_\infty$ span the nullspace of $\boldsymbol{A}$ (see (3.10)) and insert the constant solutions in space $u\,\mathbf{u}_\infty$ and $v\,\mathbf{u}_\infty$ with $\|\mathbf{u}_\infty\|_1 = 1$ as $\mathbf{u}$ and $\mathbf{v}$ in (4.25). Then the right hand sides are

$$\begin{aligned} -ku\boldsymbol{T}\mathbf{u}_\infty + \ell v \boldsymbol{T}\mathbf{u}_\infty &= 0, \\ ku\boldsymbol{T}\mathbf{u}_\infty - \ell v \boldsymbol{T}\mathbf{u}_\infty &= 0. \end{aligned} \tag{4.26}$$

Both equations in (4.26) are satisfied if $k\,u = \ell\,v$. Hence, the steady state solution is $u(\mathbf{u}_\infty, (k/\ell)\,\mathbf{u}_\infty)$, where u depends on the initial data. By mass conservation in Lemma 3.1

$$\mathbf{e}^T \mathbf{u}(0) + \mathbf{e}^T \mathbf{v}(0) = \mathbf{e}^T \mathbf{u}(t) + \mathbf{e}^T \mathbf{v}(t) = u\left(\mathbf{e}^T \mathbf{u}_\infty + (k/\ell)\,\mathbf{e}^T \mathbf{u}_\infty\right) = u(1 + k/\ell). \tag{4.27}$$

The macroscopic reaction coefficients can be regarded as time and space dependent and the macroscopic equations can be expressed without fractional derivatives. Introduce small perturbations $\delta\mathbf{u}$ and $\delta\mathbf{v}$ around the steady state in (4.25)

$$\mathbf{u}(\boldsymbol{x},t) = u\mathbf{u}_\infty + \delta\mathbf{u}(\boldsymbol{x},t), \quad \mathbf{v}(\boldsymbol{x},t) = v\mathbf{u}_\infty + \delta\mathbf{v}(\boldsymbol{x},t).$$

Then for $U = \mathbf{e}^T\,\mathbf{u} = u + \mathscr{O}(\|\delta\mathbf{u}\|)$ and $V = \mathbf{e}^T\,\mathbf{v} = v + \mathscr{O}(\|\delta\mathbf{v}\|)$ we derive

$$\begin{aligned}\frac{\partial U}{\partial t} &= \sigma^2\mathbf{e}^T\boldsymbol{T}\Delta\delta\mathbf{u} - ku\mathbf{e}^T\boldsymbol{T}\mathbf{u}_\infty - k\mathbf{e}^T\boldsymbol{T}\delta\mathbf{u} + \ell v\mathbf{e}^T\boldsymbol{T}\mathbf{u}_\infty + \ell\mathbf{e}^T\boldsymbol{T}\delta\mathbf{v} = -K'U + L'V + \mathscr{O}(\|\delta\mathbf{u}\|),\\ \frac{\partial V}{\partial t} &= \sigma^2\mathbf{e}^T\boldsymbol{T}\Delta\delta\mathbf{v} + ku\mathbf{e}^T\boldsymbol{T}\mathbf{u}_\infty + k\mathbf{e}^T\boldsymbol{T}\delta\mathbf{u} - \ell v\mathbf{e}^T\boldsymbol{T}\mathbf{u}_\infty - \ell\mathbf{e}^T\boldsymbol{T}\delta\mathbf{v} = -K'U - L'V + \mathscr{O}(\|\delta\mathbf{v}\|),\end{aligned}$$

(4.28)

where

$$\begin{aligned}K' &= k\frac{\mathbf{e}^T\boldsymbol{T}(u\mathbf{u}_\infty+\delta\mathbf{u})}{\mathbf{e}^T(u\mathbf{u}_\infty+\delta\mathbf{u})} = k\mathbf{e}^T\boldsymbol{T}\mathbf{u}_\infty + \mathscr{O}(\|\delta\mathbf{u}\|),\\ L' &= \ell\frac{\mathbf{e}^T\boldsymbol{T}(v\mathbf{u}_\infty+\delta\mathbf{v})}{\mathbf{e}^T(v\mathbf{u}_\infty+\delta\mathbf{v})} = \ell\mathbf{e}^T\boldsymbol{T}\mathbf{u}_\infty + \mathscr{O}(\|\delta\mathbf{v}\|).\end{aligned} \quad (4.29)$$

The effective macroscopic reaction coefficients are K' and L' when $t \gg 0$, cf. (3.36) with $\boldsymbol{K}_1 = k\boldsymbol{T}$.

With more general $\boldsymbol{K}$ and $\boldsymbol{L}$ in (3.21), the structure of the equations is the same as in (4.25) but there is no corresponding macroscopic FPDE. For example, let $\boldsymbol{K} = \boldsymbol{T}\,\mathbf{e}\,\mathbf{f}^T\boldsymbol{T}$ and $\boldsymbol{L} = \boldsymbol{T}\,\mathbf{e}\,\mathbf{g}^T\boldsymbol{T}$ with $\mathbf{f}^T\boldsymbol{T}\,\mathbf{e} > 0$ and $\mathbf{g}^T\boldsymbol{T}\,\mathbf{e} > 0$. Then $\boldsymbol{K}_1 = k\boldsymbol{T}$ with $k = \mathbf{f}^T\mathbf{T}\,\mathbf{e}$ and $\boldsymbol{L}_1 = \ell\boldsymbol{T}$ with $\ell = \mathbf{g}^T\mathbf{T}\,\mathbf{e}$. The equations for $\mathbf{u}$ and $\mathbf{v}$ are

$$\begin{aligned}\frac{\partial\mathbf{u}}{\partial t} &= \boldsymbol{T}\left(\sigma^2\Delta\mathbf{u} - k\mathbf{u} + g\mathbf{e}^T\boldsymbol{T}\mathbf{v}\right) + \boldsymbol{A}\,\mathbf{u},\\ \frac{\partial\mathbf{v}}{\partial t} &= \boldsymbol{T}\left(\sigma^2\Delta\mathbf{v} + f\mathbf{e}^T\boldsymbol{T}\mathbf{u} - \ell\mathbf{v}\right) + \boldsymbol{A}\,\mathbf{v}.\end{aligned} \quad (4.30)$$

The macroscopic waiting time for the reactions is not obvious in this case.

As in (4.24), let one state i be transformed to the same state i and choose the reaction rates to be constant for all states $K_{ii} = k$ and $L_{ii} = \ell$ with $\tau_i = 1$ in Table 3.1. Insert $\boldsymbol{K} = k\boldsymbol{I}$ and $\boldsymbol{L} = \ell\boldsymbol{I}$ into (3.22) and (3.23) to obtain

$$\begin{aligned}\frac{\partial\mathbf{u}}{\partial t} &= \sigma^2\boldsymbol{T}\Delta\mathbf{u} + \boldsymbol{A}\,\mathbf{u} - k\mathbf{u} + \ell\mathbf{v},\\ \frac{\partial\mathbf{v}}{\partial t} &= \sigma^2\boldsymbol{T}\Delta\mathbf{v} + \boldsymbol{A}\,\mathbf{v} + k\mathbf{u} - \ell\mathbf{v}.\end{aligned} \quad (4.31)$$

Only the diffusion has different waiting times in different states while the waiting times for the reactions are the same in all states. Let $\boldsymbol{M}_r$ and $\boldsymbol{M}_d$ be the reaction matrix and the operator for the diffusion and the change of state in (4.31)

$$M_r=\begin{pmatrix} -k\boldsymbol{I} & \ell\boldsymbol{I} \\ k\boldsymbol{I} & -\ell\boldsymbol{I} \end{pmatrix},\quad M_d=\begin{pmatrix} \sigma^2\boldsymbol{T}\Delta+\boldsymbol{A} & 0 \\ 0 & \sigma^2\boldsymbol{T}\Delta+\boldsymbol{A} \end{pmatrix}. \tag{4.32}$$

There is a transformation from (4.14) via (4.15) to (4.17). Since $\boldsymbol{M}_r$ and $\boldsymbol{M}_d$ commute in (4.32), there is a similar transformation for (4.31). As in (4.14), $\mathbf{e}^T\mathbf{u}$ and $\mathbf{e}^T\mathbf{v}$ approximate model II in (2.30).

If the diffusion rate is independent of the state but the waiting time for the reactions depends on the state in (4.24) then $D_{ii}=\sigma^2$ in (3.13), $K_{ii}=k/\tau_i$ and $L_{ii}=\ell/\tau_i$. The mesoscopic model is

$$\begin{aligned} \tfrac{\partial \mathbf{u}}{\partial t}&=\boldsymbol{T}\,(-k\mathbf{u}+\ell\mathbf{v})+\boldsymbol{A}\mathbf{u}+\sigma^2\Delta\mathbf{u}, \\ \tfrac{\partial \mathbf{v}}{\partial t}&=\boldsymbol{T}\,(k\mathbf{u}-\ell\mathbf{v})+\boldsymbol{A}\mathbf{v}+\sigma^2\Delta\mathbf{v}. \end{aligned} \tag{4.33}$$

We have the ordinary diffusion but the reactions behave anomalously at the macroscopic level with the waiting time $\psi_i(t)$ depending on the state.

4.3.3. Bimolecular reactions—We consider three species A, B and C in N different internal states and the chemical reactions

$$A_i+B_i\underset{\lambda_i}{\overset{\kappa_i}{\rightleftharpoons}}C_i,\quad i=1,\ldots,N. \tag{4.34}$$

This is a less general set of reactions than in (3.42) in that only molecules in the same internal state react with each other. The internal states reaction-diffusion system (3.43)–(3.45) is then modified as follows for state i

$$\begin{aligned} \tfrac{\partial u_i}{\partial t}&=D_i\Delta u_i+\sum_{j=1}^{N}A_{ij}u_j-K_{iii}u_iv_i+L_{iii}w_i, \\ \tfrac{\partial v_i}{\partial t}&=D_i\Delta v_i+\sum_{j=1}^{N}A_{ij}v_j-K_{iii}u_iv_i+L_{iii}w_i, \\ \tfrac{\partial w_i}{\partial t}&=D_i\Delta w_i+\sum_{j=1}^{N}A_{ij}w_j+K_{iii}u_iv_i-L_{iii}w_i. \end{aligned} \tag{4.35}$$

The reaction coefficients in (4.35) are chosen to be $K_{iii}=k/\tau_i$ and $L_{iii}=\ell/\tau_i$. Then at state i

$$\begin{aligned}
\frac{\partial u_i}{\partial t} &= \frac{1}{\tau_i}\left(\sigma^2 \Delta u_i - k u_i v_i + \ell w_i\right) + \sum_{j=1}^{N} A_{ij} u_j, \\
\frac{\partial v_i}{\partial t} &= \frac{1}{\tau_i}\left(\sigma^2 \Delta v_i - k u_i v_i + \ell w_i\right) + \sum_{j=1}^{N} A_{ij} v_j, \\
\frac{\partial w_i}{\partial t} &= \frac{1}{\tau_i}\left(\sigma^2 \Delta w_i + k u_i v_i - \ell w_i\right) + \sum_{j=1}^{N} A_{ij} w_j.
\end{aligned} \tag{4.36}$$

The reactions and the diffusion have the same waiting time in each state in (4.36) as in (4.25). Hence, the equations will approximate model **I** at the macroscopic level in (2.31). By letting $K_{iii} = k$ and $L_{iii} = \ell$ independent of the internal state in (4.35), equations similar to the model II equations (4.31) are obtained but there is no transformation (4.15) with a constant $\boldsymbol{K}_1$.

We have found that certain annihilation, monomolecular, and bimolecular reactions at the mesoscopic level have a macroscopic counterpart as a FPDE. Furthermore, the long time behavior of the reactions tends to that of ordinary reactions without internal states. This will be confirmed in numerical examples in the next section.

5. Numerical experiments

Since this paper focuses on the mesoscopic approximation of subdiffusion, we will investigate only the 1D reaction-diffusion system. However, the strategy proposed here can be extended straightforwardly to 2D and 3D geometries.

The integration of the internal states systems (3.13), (3.22)–(3.23) and (3.43)–(3.45) is detailed in Section 5.1. The general configuration of the numerical experiments is introduced in Section 5.2: physical parameters, numerical parameters of the discretization, and initial conditions. Then the numerical experiments are described. In Section 5.3, both the diffusive approximation introduced in Section 4.1 and the numerical method introduced in Section 5.1 are verified in comparisons. In Sections 5.4 and 5.5, the method is applied to both model I and model II for reactive systems. The differences between the two models are also illustrated. Finally examples of bimolecular reactions, for which no analytical solutions are available, are presented in Section 5.6.

5.1. Numerical modeling

In order to integrate the internal states systems (3.13), (3.22)–(3.23) and (3.43)–(3.45), a uniform grid is introduced with mesh size h and time step Δt. The approximation of the exact solution $\mathbf{u}$ is denoted by $\mathbf{u}_j^n$ at x_j and t^n. The Laplace operators involved in the internal states systems (3.13), (3.22)–(3.23) and (3.43)–(3.45) are discretized using second order centered finite differences as in (3.12):

$$\Delta \mathbf{u} \equiv \frac{\partial^2 \mathbf{u}}{\partial \boldsymbol{x}^2} = \frac{1}{h^2} \left(\mathbf{u}_{j+1} - 2\mathbf{u}_j + \mathbf{u}_{j-1} \right). \quad (5.1)$$

The jump coefficients in (3.12) are $\lambda_{j1} = \lambda_{j2} = 1/h^2$ and $\lambda_j = 2/h^2$. The resulting system of ODEs in time can be written

$$\frac{\partial \mathbf{u}_j}{\partial t} = F_\ell \left(\mathbf{u}_{j-1}, \mathbf{u}_j, \mathbf{u}_{j+1} \right) + F_{n\ell} \left(\mathbf{u}_j \right), \quad (5.2)$$

where F_ℓ contains the discrete Laplacian and the linear reaction terms and the $F_{n\ell}$ the nonlinear reaction terms. The system of ODEs (5.2) is discretized using the following finite difference scheme

$$\frac{\mathbf{u}_j^{n+1} - \mathbf{u}_j^n}{\Delta t} = \frac{1}{2} \left(F_\ell \left(\mathbf{u}_{j-1}^{n+1}, \mathbf{u}_j^{n+1}, \mathbf{u}_{j+1}^{n+1} \right) + F_\ell \left(\mathbf{u}_{j-1}^n, \mathbf{u}_j^n, \mathbf{u}_{j+1}^n \right) \right) + F_{n\ell} \left(\mathbf{u}_j^n \right). \quad (5.3)$$

In the case of an annihilation process and a monomolecular reaction, there is no nonlinear reaction term. Hence, $F_{n\ell}$ is zero, and (5.3) reduces to the Crank-Nicholson scheme. It is second-order accurate in space and time and it is unconditionally stable. In the case of a bimolecular reaction, because of the nonlinearities, the method is first order accurate in time.

5.2. Configurations

In order to demonstrate the ability of the present method to be applied to a wide range of problems, we numerically test in Section 5.3 two different sets of parameters, given in Table 5.1. Then only the first set of parameters is used in Sections 5.4, 5.5 and 5.6. In our code, a, K_a, t_{min}, t_{max} are input parameters, and σ^2, τ, N, τ_i, μ_i are ouput parameters. The quadrature coefficients τ_i and μ_i in (4.7) are determined by nonlinear optimization [2] and the corresponding model error ε_{mod} (4.5) is also given in the table.

The computational domain is $\Omega = [-1, 1]$ in Figure 5.1 and $[-10, 10]$ in Figure 5.2, is discretized with $N_x = 128$ grid points. Neumann boundary conditions are used. As the initial condition, we use a Gaussian $g(x)$, centered at point (0, 0) and of variance $\sigma_g^2 = 10^{-3}$, rather than a Dirac distribution to avoid spurious numerical artifacts. Moreover, each internal state is initialized by the weight μ_ℓ

5.3. Subdiffusion

The aim of the first test is to check the accuracy of the numerical method above when no reaction occurs. The following initial conditions are used

$$\mathbf{u}(x, 0) = \boldsymbol{\mu}\, g(x). \quad (5.4)$$

Figure 5.1 compares the numerical solution $U = \mathbf{e}^T \mathbf{u}$ obtained with the PDEs in the internal state diffusion system (3.13) with the analytical solution of the FPDE (2.16). Figure 5.1-(a) corresponds to the first set of parameters, given in Table 5.1, at time $t_1 = 5 \cdot 10^{-3}$ s and Figure 5.1-(b) corresponds to the second set of parameters at time $t_2 = 1.5 \cdot 10^{-1}$ s. Note in Table 5.1 that the macroscopic parameters α and K_α, involved in (2.11), are the same for both sets of parameters. Consequently, they approximate the same macroscopic FPDE, but in two different time intervals $[t_{min}, t_{max}]$. In both cases, the final time of the simulation in Figure 5.1 is inside this interval. Excellent agreement is found between the two solutions.

Two errors should be mentioned here: the modeling error, defined as the difference between the internal states diffusion model and the FPDE model, and the numerical error ε_{num}, resulting from the numerical discretization of the internal states diffusion system. The modeling error is dependent on ε_{mod} in (4.5). The error ε_{mod} is given in Table 5.1 and the total error ε_{tot} is measured in Figure 5.1 as the difference between the numerical solution obtained with the PDE model (red circles) with the analytical solution obtained with the FPDE model (black solid line). In Figure 5.1-(a) $\varepsilon_{tot} \simeq 2.33 \cdot 10^{-2}$ and in Figure 5.1-(b) $\varepsilon_{tot} \simeq 3.65 \cdot 10^{-2}$.

Figure 5.2 shows the mean square displacement divided by the time, which is constant for ordinary diffusion, see (2.8). According to the analysis in Section 4.2, ordinary diffusion is observed for $t \ll \min_{\ell=1,\dots,N} \tau\ell$ and for $t \gg \max_{\ell=1,\dots,N} \tau\ell$ For intermediate times, the diffusion is anomalous by construction, cf. Section 4.1. The subdiffusive exponent α is measured by linear regression: $\alpha \simeq 0.4997$ in Figure 5.2-(a) and $\alpha \simeq 0.5454$ in Figure 5.2-(b). In both cases the measured subdiffusive exponent is close to the theoretical one.

5.4. Annihilation process

The purpose of the second test is to investigate the accuracy of the numerical method in the case of an annihilation process. Two different models are possible in Section 2.3.1

$$\begin{aligned} &\text{Model I} \quad A_i \xrightarrow{k/\tau_i} \varnothing, \\ &\text{Model II} \quad A_i \xrightarrow{k} \varnothing. \end{aligned} \tag{5.5}$$

The reaction coefficient k used in the simulations and the corresponding macroscopic reaction rate k_* (4.13)–(4.16) are given in Table 5.2. The rate k has been chosen such that the two models have the same macroscopic reaction rates in (4.13) and (4.16). Note the order-of-magnitude difference between the value of k in model I and II, which is explained by the fact that the units of k and k_* are are different. The initial conditions are the same as in the previous test. Figure 5.3 compares the numerical solution $U = \mathbf{e}^T \mathbf{u}$ obtained with the internal state reaction-diffusion system (4.11) with the analytical solutions of the FPDEs in (2.22) and (2.26) at time $t_1 = 10^{-2}$ s. For both models, there is excellent agreement between the two solutions. The analytical solution is also given in the case where no reaction occurs ($k = 0$). For a small macroscopic reaction rate (first run, top of Figure 5.3), no reaction takes place yet in the case of model II. For large macroscopic reaction rate (second run, bottom of

Figure 5.3), all particles have disappeared in model I. The differences between the two models are clearly illustrated in Figure 5.3.

The time development of k' (4.22) is plotted in Figure 5.4. In model I (first run in Table 5.2), k' is almost constant at small t and at large t, meaning that the kinetics is ordinary there but at intermediate t k' varies in time implying that the kinetics is anomalous. This is illustrated in Figure 5.5, where the time evolution of the total amount of A, i.e. $\bar{U}$ in (4.21), is found. Exponential decay characterizing ordinary kinetics is observed for $t < t_{min}$ and $t > t_{max}$. The exponential parameters are measured by linear regression in Figure 5.5 resulting in $k'(0) \approx 28.97$ and $k'_\infty \approx 674.08$ when $t \to \infty$. In both cases, the measured exponential parameter is close to the theoretical one in (4.22) (blue values in Figure 5.4). For $t_{min} < t < t_{max}$, $\bar{U}$ does not decrease exponentially. In model II (second run in Table 5.2), Figure 5.4 shows that $k' = k$ does not depend on time and exponential decay is observed for all times in Figure 5.5. The measured exponential parameter $k' \approx 50.00$ is close to the theoretical one. These observations agree with the analysis in Sections 2.3.1 and 4.3.1.

5.5. Monomolecular reaction

The numerical method is here applied to monomolecular reversible reactions. Consider the reactions

$$\begin{aligned} &\text{Model I} \quad A_i \underset{\ell/\tau_i}{\overset{k/\tau_i}{\rightleftharpoons}} B_i, \\ &\text{Model II} \quad A_i \underset{\ell}{\overset{k}{\rightleftharpoons}} B_i, \end{aligned} \tag{5.6}$$

where the coefficients k and ℓ used in the simulations are given in Table 5.3. As discussed in Section 4.3.2, these cases correspond to the macroscopic FPDEs (2.27) and (2.30) with macroscopic reaction rates k_* and ℓ_* given in Table 5.3. The rates k and ℓ have been chosen such that the two models have the same macroscopic reaction rates k_* and ℓ_* and the same steady states. Figure 5.6 then illustrates the differences between the two models. The following initial conditions are used

$$\mathbf{u}(x,0) = \mathbf{v}(x,0) = \boldsymbol{\mu} g(x). \tag{5.7}$$

Figure 5.6 compares the numerical solutions of $U = \mathbf{e}^T\mathbf{u}$ and $V = \mathbf{e}^T\mathbf{v}$ obtained with the internal state reaction-diffusion system (3.22)–(3.23) with the analytical solutions of the FPDEs in Section 2.3.2. The difference between the models is obvious in Figure 5.6-(a) corresponding to model I at time $t_1 = 10^{-2}$ s and Figure 5.6-(b) with the model II at the same time. For both models, good agreement is found between the mesoscopic PDE and the macroscopic FPDE solutions.

The numerical solution of the internal states reaction-diffusion system at time $t_2 = 10$ s is depicted in Figure 5.7 when the steady state is reached. We note that the numerical values of the steady states are close to the theoretical ones, given by the kernel of the matrix $\boldsymbol{B}$ in

(3.28). Using (3.36), the equivalent reactions rates k_{eq} and ℓ_{eq} are computed, cf Table 5.3, and the property $k_{eq}\, u_\infty = \ell_{eq}\, v_\infty$ when $t \to \infty$ in (3.40) and (3.41) is verified.

5.6. Bimolecular reaction

The purpose of the last example is to establish whether the numerical methods presented in this paper can be used to handle more complex reactions. As an example, we consider the following bimolecular reversible reactions

$$\begin{aligned} &\text{Reaction I} \quad A_i + B_i \underset{\ell/\tau_i}{\overset{k/\tau_i}{\rightleftharpoons}} C_i, \\ &\text{Reaction II} \quad A_i + B_j \underset{\ell/\tau_k}{\overset{\frac{k}{2}\left(\frac{1}{\tau_i}+\frac{1}{\tau_j}\right)}{\rightleftharpoons}} C_k, \\ &\text{Reaction III} \quad A_i + B_i \underset{\ell}{\overset{k}{\rightleftharpoons}} C_i. \end{aligned} \tag{5.8}$$

The reaction rates are found in Table 3.1 with τ_{ij} for reaction II chosen as in (3.7) with $\theta = 1/2$ since A and B diffuse with the same speed. The rates of reactions I and III are as in model I and II in Sections 4.3.1 and 4.3.2 but reaction II is more general. The initial conditions are

$$\mathbf{u}\,(x,0) = \frac{1}{2}\boldsymbol{\mu} g(x), \quad \mathbf{v}\,(x,0) = \frac{1}{4}\boldsymbol{\mu} g(x), \quad \mathbf{w}\,(x,0) = \boldsymbol{\mu} g(x). \tag{5.9}$$

The numerical solutions $U = \mathbf{e}^T\mathbf{u}$, $V = \mathbf{e}^{\mathrm{T}}\mathbf{v}$ and $W = \mathbf{e}^T\mathbf{w}$ of the internal states reaction-diffusion system are shown in Figure 5.6 at time $t_1 = 10^{-2}$ s (top) and at time $t_2 = 10$ s (bottom) when the steady state is reached. For reaction I, we expect that the internal states model in (4.36) approximates the macroscopic FPDE model I (2.31). No analytical solution of the FPDE is available in this case. For reaction II and reaction III, the macroscopic level with summation over the internal states is not so easily expressed as a FPDE. Using (3.48)–(3.52), the equivalent reactions rates k_{eq} and ℓ_{eq} are computed in Table 5.4 and the property $k_{eq}\, u_\infty\, v_\infty = \ell_{eq}\, w_\infty$ when $t \to \infty$ in (3.53)–(3.55) is verified.

6. Conclusion

A numerical method is presented here for simulating fractional-in-time reaction-diffusion equations. A diffusive representation transforms the function $\frac{1}{t^{\alpha+1}}$, involved in the mesoscopic CTRW on a lattice, into a continuum of decreasing exponentials, approximated by quadrature formulae. The CTRW model is then replaced by an approximation, much more tractable numerically. Contrary to the approach used in [38], the coefficients of the diffusive approximation are determined by a nonlinear optimization procedure, leading to a smaller number of internal states. At the macroscopic level, the internal states diffusion system thus obtained corresponds to the fractional diffusion equation in a chosen time interval. In contrast to the FPDE model, the diffusion in the internal states model is ordinary

at small and large times, but it is anomalous at intermediate times. This behavior can also be observed in crowded systems of hard-spheres due to caging effects, and hence the model used herein may actually be a better model for microscopic crowding than the traditional FPDE description.

The internal states model for diffusion in [38] is here extended to account for chemical reactions. On the macroscopic FPDE level, two different models for reactions with subdiffusion are investigated. In model I the fractional derivative acts on both on the standard diffusion term and the reaction term, whereas in model II the fractional derivative acts only on the diffusion term. Both macroscopic FPDE models correspond to a mesoscopic internal states model with particular reaction coefficients. However, the opposite is not true; mesoscopic models with general reactions may not have a simple interpretation at the macroscopic level. In model I, the reactions are subdiffusion controlled, that is the reaction kinetics is ordinary at small and large times, whereas it is anomalous at intermediate times. In model II, the reaction kinetics is ordinary for all times. Which one of these models provides a better description of a reaction system subject to subdiffusion does not have a simple answer. In either case, the present work provids a theoretical foundation for practical and efficient mesoscopic simulations.

Acknowledgments

This work was supported by the Swedish strategic research programme eSSENCE, the UPMARC Linnaeus center of Excellence, and the NIH grant for StochSS with number 1R01EB014877-01.

Appendix A. Special functions

The Fox-H function is defined as a Mellin-Barnes integral [12]

$$H_{p,q}^{m,n}\left[z\middle|\begin{matrix}(a_1,A_1) & (a_2,A_2) & \cdots & (a_p,A_p)\\ (b_1,B_1) & (b_2,B_2) & \cdots & (b_q,B_q)\end{matrix}\right]=\frac{1}{2i\pi}\oint_L \frac{\prod_{j=1}^{m}\Gamma\left(b_j-B_j s\right)\times\prod_{j=1}^{n}\Gamma\left(1-a_j+A_j s\right)}{\prod_{j=m+1}^{q}\Gamma\left(1-b_j+B_j s\right)\times\prod_{j=n+1}^{p}\Gamma\left(a_j-A_j s\right)}z^s ds,$$

(A.1)

where L is a certain contour separating the poles of the two factors in the numerator. The special case for which the Fox-H function reduces to the Meijer-G function is $A_j = B_k = C$, $C > 0$ for $j = 1, \cdots, p$ and $k = 1, \cdots, q$ [47]

$$H_{p,q}^{m,n}\left[z\middle|\begin{matrix}(a_1,C) & (a_2,C) & \cdots & (a_p,C)\\ (b_1,C) & (b_2,C) & \cdots & (b_q,C)\end{matrix}\right]=\frac{1}{2i\pi C}\oint_L \frac{\prod_{j=1}^{m}\Gamma(b_j-s)\times\prod_{j=1}^{n}\Gamma(1-a_j+s)}{\prod_{j=m+1}^{q}\Gamma(1-b_j+s)\times\prod_{j=n+1}^{p}\Gamma(a_j-s)}z^{s/C}ds,$$
$$=\frac{1}{C}G_{p,q}^{m,n}\left[z^{1/C}\middle|\begin{matrix}a_1,\cdots,a_p\\ b_1,\cdots,b_p\end{matrix}\right].$$

(A.2)

References

1. Berkowitz Y, Edery Y, Scher H, Berkowitz B. Fickian and non-Fickian diffusion with bimolecular reactions. Phys Rev E. 2013; 87:032812.
2. Blanc, E. Approximation of the diffusive representation by decreasing exponential functions. Department of Information Technology, Uppsala University; 2015. Tech Rep 2015-009
3. Blinov ML, Faeder JR, Goldstein B, Hlavacek WS. BioNetGen: software for rule-based modeling of signal transduction based on the interactions of molecular domains. Bioinformatics. 2004; 20(17): 3289–3291. [PubMed: 15217809]
4. Bray D. Molecular prodigality. Science. 2003; 299(5610):1189–1190. [PubMed: 12595679]
5. Caputo M. Linear models of dissipation whose Q is almost frequency independent, part 2. Geophys J R Astr Soc. 1967; 13:529–539.
6. Collins FC, Kimball GE. Diffusion-controlled reaction rates. J Colloid Sci. 1949; 4:425–437.
7. Desch W, Miller R. Exponential stabilization of Volterra integral equations with singular kernels. J Int Eq Appl. 1988; 1(3):397–433.
8. Drawert B, Engblom S, Hellander A. URDME: a modular framework for stochastic simulation of reaction-transport processes in complex geometries. BMC Syst Biol. 2012; 6(1):76. [PubMed: 22727185]
9. Endy D, Brent R. Modelling cellular behaviour. Nature. 2001; 409:391–395. [PubMed: 11201753]
10. Engblom S, Ferm L, Hellander A. Lötstedt, P. Simulation of stochastic reaction-diffusion processes on unstructured meshes. SIAM J Sci Comput. 2009; 31:1774–1797.
11. Fange D, Elf J. Noise induced Min phenotypes in E. coli. PLoS Comput Biol. 2006; 2(6):e80. [PubMed: 16846247]
12. Fox C. The G and H functions as symmetrical Fourier kernels. Trans Am Math Soc. 1961; 98(3): 395–429.
13. Gillespie DT. A general method for numerically simulating the stochastic time evolution of coupled chemical reactions. J Comput Phys. 1976; 22(4):403–434.
14. Gillespie DT. Master equations for random walks with arbitrary pausing time distributions. Phys Lett. 1977; 64A:22–24.
15. Glöckle W, Nonnenmacher T. A fractional calculus approach to self-similar protein dynamics. Biophys J. 1995; 68(1):46–53. [PubMed: 7711266]
16. Glöckle WG, Nonnenmacher TF. Fractional integral operators and Fox functions in the theory of viscoelasticity. Macromol. 1991; 24(24):6426–6434.
17. Haddar H, Li JR, Matignon D. Efficient solution of a wave equation with fractional-order dissipative terms. J Comput Appl Math. 2010; 234(6):2003–2010.
18. Hattne J, Fange D, Elf J. Stochastic reaction-diffusion simulation with MesoRD. Bioinformatics. 2005; 21(12):2923–2924. [PubMed: 15817692]
19. Haus JW, Kehr KW. Diffusion in regular and disordered lattices. Phys Rep. 1987; 150(5):263–406.

20. Heleschewitz, D. PhD thesis. ENST; France: 2000. Analyse et simulation de système différentiels fractionnaires et pseudo-différentiels linéaires sous représentation diffusive.
21. Henry BJ, Langlands TAM, Wearne SL. Anomalous diffusion with linear reaction dynamics: From continuous time random walks to fractional reaction-diffusion equations. Phys Rev E. 2006; 74:031116.
22. Hepburn I, Chen W, Wils S, Schutter E. STEPS: efficient simulation of stochastic reaction-diffusion models in realistic morphologies. BMC Syst Biol. 2012; 6(35)
23. Höfling F, Franosch T. Anomalous transport in the crowded world of biological cells. Rep Progr Phys. 2013; 76:046602.
24. Hornung G, Berkowitz B, Barkai N. Morphogen gradient formation in a complex environment: An anomalous diffusion model. Phys Rev E. 2005; 72:041916.
25. Jeon JH, Tejedor V, Burov S, Barkai E, Selhuber-Unkel C, Berg-Sørensen K, Oddershede L, Metzler R. In Vivo anomalous diffusion and weak ergodicity breaking of lipid granules. Phys Rev Lett. 2011; 106:048103. [PubMed: 21405366]
26. van Kampen, NG. Stochastic Processes in Physics and Chemistry. 2nd. Elsevier; Amsterdam: 2004.
27. Kenkre VM, Montroll EW, Shlesinger MF. Generalized master equations for continuous-time random walks. J Stat Phys. 1973; 9(1):45–50.
28. Klafter, J., Lim, S., Metzler, R. Fractional Dynamics: Recent Advances. World Scientific; 2012.
29. Kurtz TG. Solutions of ordinary differential equations as limits of pure jump Markov processes. J Appl Prob. 1970; 7:49–58.
30. Kusumi A, Nakada C, Ritchie K, Murase K, Suzuki K, Murakoshi H, Kasai RS, Kondo J, Fujiwara T. Paradigm shift of the plasma membrane concept from the two-dimensional continuum fluid to the partitioned fluid: High-speed single-molecule tracking of membrane molecules. Annu Rev Biophys Biomol Struct. 2005; 34:351–378. [PubMed: 15869394]
31. Lawson MJ, Drawert B, Khammash M, Petzold L, Yi TM. Spatial stochastic dynamics enable robust cell polarization. PLoS Comput Biol. 2013; 9(7):e1003139. [PubMed: 23935469]
32. Lomholt MA, Zaid IM, Metzler R. Subdiffusion and weak ergodicity breaking in the presence of a reactive boundary. Phys Rev Lett. 2007; 98:200603. [PubMed: 17677681]
33. Lopez CF, Muhlich JL, Bachman JA, Sorger PK. Programming biological models in Python using PySB. Molecular Systems Biology. 2013; 9(1)
34. Mainardi F, Raberto M, Gorenflo R, Scalas E. Fractional calculus and continuous-time finance II: the waiting-time distribution. Physica A: Stat Mech Appl. 2000; 287(3–4):468–481.
35. Marquez-Lago TT, Leier A, Burrage K. Anomalous diffusion and multifractional Brownian motion: simulating molecular crowding and physical obstacles in systems biology. IET Syst Biol. 2012; 6(4):134–142. [PubMed: 23039694]
36. Metzler R, Klafter J. The random walk's guide to anomalous diffusion: a fractional dynamics approach. Phys Rep. 2000; 339(1):1–77.
37. Miller, KS., Ross, B. An Introduction to the Fractional Calculus and Fractional Differential Equations. Wiley; New-York: 1993.
38. Mommer MS, Lebiedz D. Modeling subdiffusion using reaction diffusion systems. SIAM J Appl Math. 2009; 70(1):112–132.
39. Montroll EW, Weiss GH. Random walks on lattices. II. J Math Phys. 1965; 6(2):167–181.
40. Saxton MJ. Chemically limited reactions on a percolation cluster. J Chem Phys. 2002; 116:203–208.
41. Saxton MJ. A biological interpretation of transient anomalous subdiffusion. I. Qualitative model. Biophys J. 2007; 92:1178–1191. [PubMed: 17142285]
42. Seki K, Wojcik M, Tachiya M. Fractional reaction-diffusion equation. The Journal of chemical physics. 2003; 119(4):2165–2170.
43. Shkilev VP. Effect of microscopic inhomogeneity of the medium on the reaction-diffusion front velocity. J Exp Theor Phys. 2009; 108(2):356–363.
44. Shkilev VP. Comment on "Anomalous versus slowed-down Brownian diffusion in the ligand-binding equilibrium". Biophys J. 2014; 106:2541–2543. [PubMed: 24896134]

45. Sokolov IM, Schmidt MGW. Sagués, F. Reaction-subdiffusion equations. Phys Rev E. 2006; 73:031102.

46. Soula H, Caré B, Beslon G, Berry H. Anomalous versus slowed-down Brownian diffusion in the ligand-binding equilibrium. Biophys J. 2013; 105:2064–2073. [PubMed: 24209851]

47. Srivastava, H., Manocha, H. A treatise on generating functions. E. Horwood; 1984. Ellis Horwood Series in Mathematics and its Applications

48. Staffans OJ. Well-posedness and stabilizability of a viscoelastic equation in energy space. Trans Amer Math Soc. 1994; 345(2):527–575.

49. Stefan MI, Bartol TM, Sejnowski TJ, Kennedy MB. Multi-state modeling of biomolecules. PLoS Comput Biol. 2014; 10(9):e1003844. [PubMed: 25254957]

50. Sturrock M, Hellander A, Aldakheel S, Petzold L, Chaplain M. The role of dimerisation and nuclear transport in the Hes1 gene regulatory network. Bull Math Biol. 2013:1–33.

51. Yadav A, Horsthemke W. Kinetic equations for reaction-subdiffusion systems: Derivation and stability analysis. Phys Rev E. 2006; 74:066118.

52. Yang H, Luo G, Karnchanaphanurach P, Louie TM, Rech I, Cova S, Xun L, Xie XS. Protein conformational dynamics probed by single-molecule electron transfer. Science. 2003; 302(5643): 262–266. [PubMed: 14551431]

53. Yuste SB, Acedo L, Lindenberg K. Reaction front in an A + B → C reaction-subdiffusion process. Phys Rev E. 2004; 69:036126.

54. Yuste, SB., Lindenberg, K., Ruiz-Lorenzo, JJ. Subdiffusion limited reactions. In: Klages, R.Radons, G., Sokolov, IM., editors. Anomalous Transport: Foundations and Applications. Weinheim: Wiley-VCH; 2007. p. 3-33.

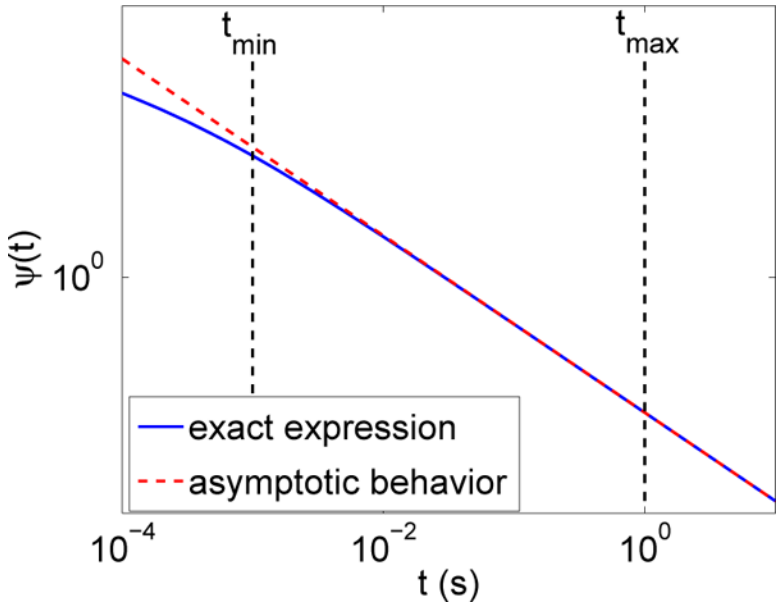

Fig. 4.1.

Section 4.1. Waiting time PDF (2.9) (blue solid line), and its asymptotic expansion (4.1) (red dotted line). The scales are logarithmic on both axes.

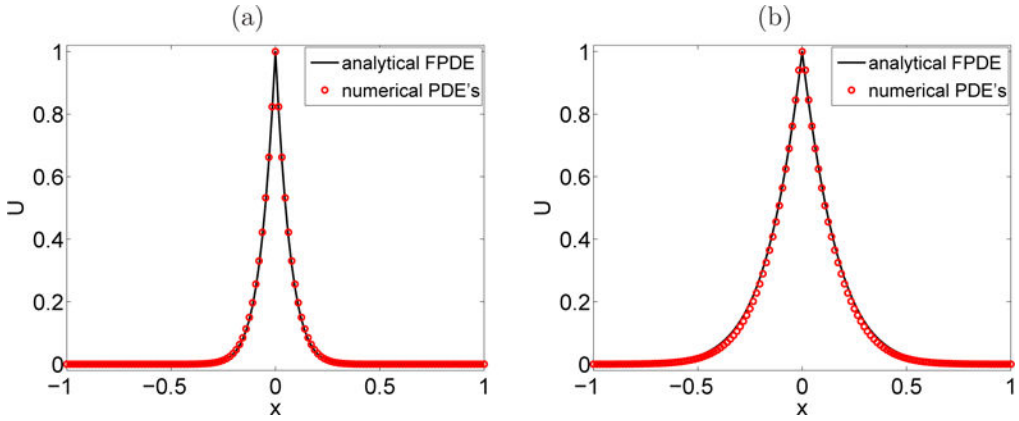

Fig. 5.1.

Section 5.3. Comparison between the numerical values (circle) and the analytical values (solid line) of the concentration $U = \mathbf{e}^T \mathbf{u}$ of A. (a): Set 1 of parameters at $t_1 = 5 \cdot 10^{-3}$ s, (b): Set 2 of parameters at $t_2 = 1.5 \cdot 10^{-1}$ s.

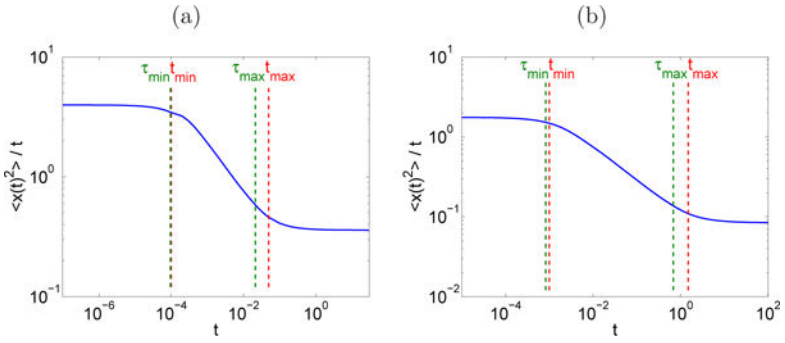

Fig. 5.2.

Section 5.3. Mean square displacement as a function of time. (a): Parameters set 1, (b): Parameters set 2. The scales are logarithmic on both axes.

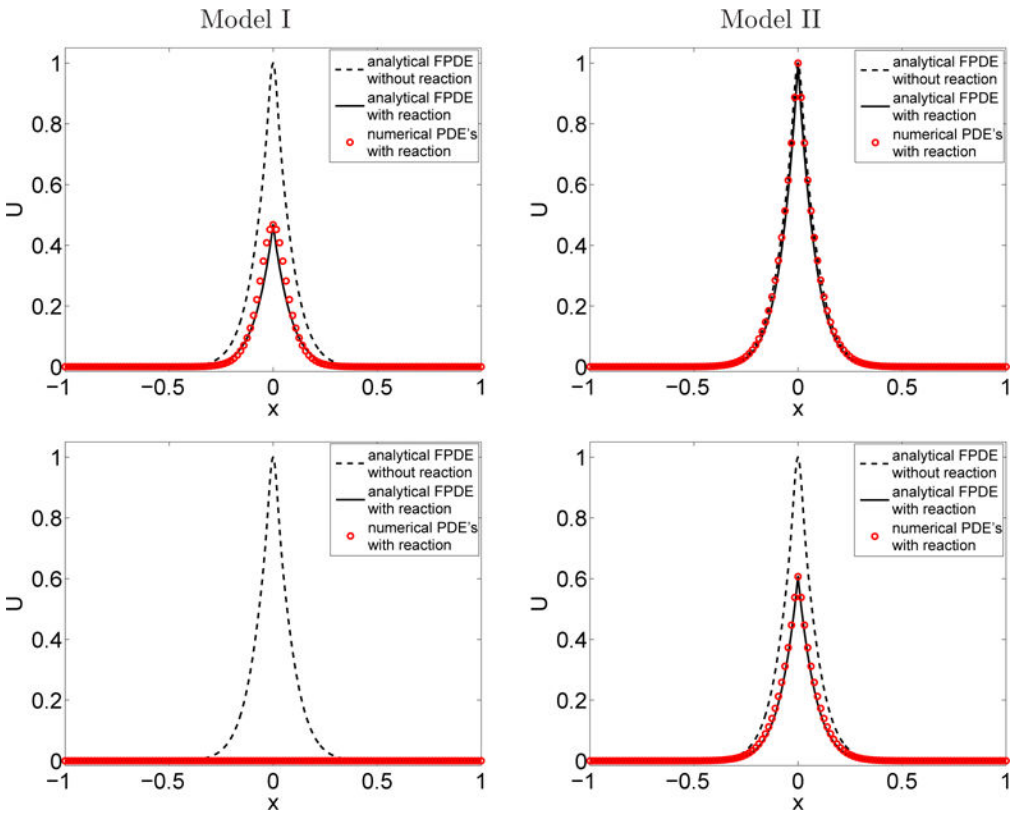

Fig. 5.3.

Section 5.4 Comparison between the numerical values (circles) and the analytical values (black line) of the conecntration $U = \mathbf{e}^T \mathbf{u}$ of A at time $t = 10^{-2}$ s. Top: First run, bottom: Second run.

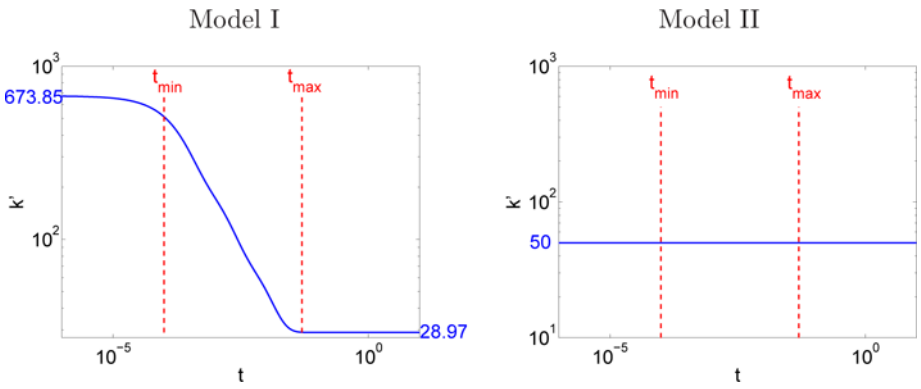

Fig. 5.4.

Section 5.4 k' in (4.22) in terms of time. Left: Model I, right: Model II. The scales are logarithmic on both axes.

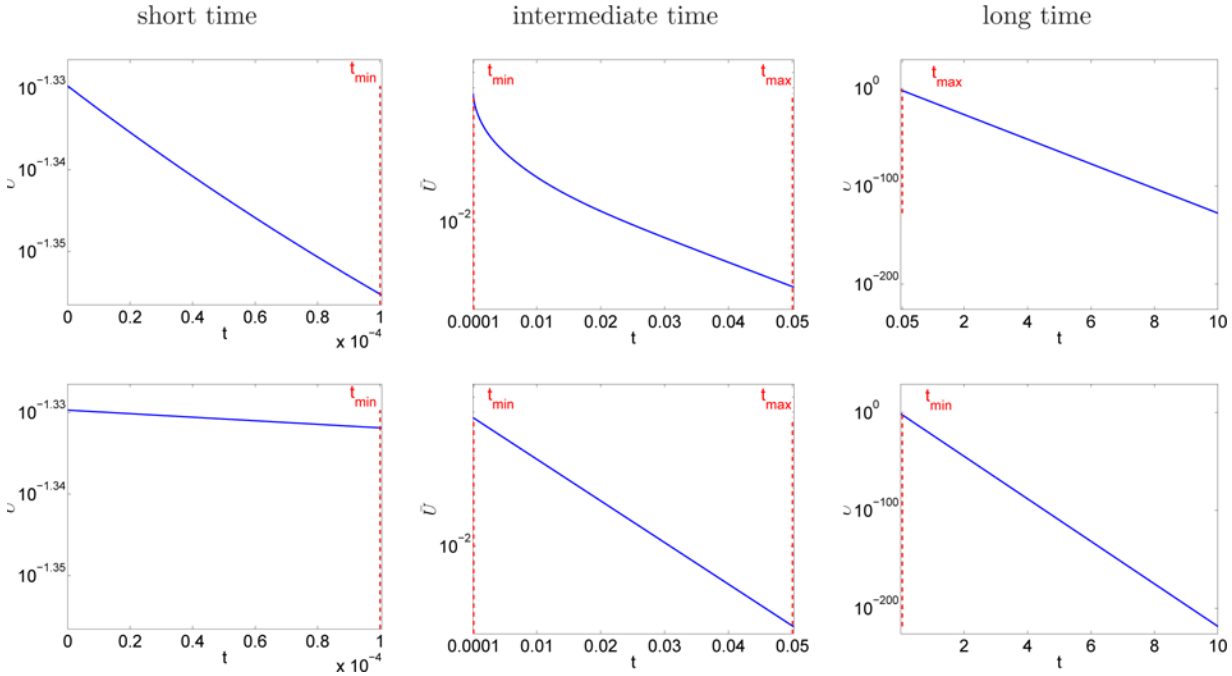

Fig. 5.5.

Section 5.4. Total amount of A (4.21) in terms of time. Upper: Model I, lower: Model II. The scale is logarithmic on the y axis.

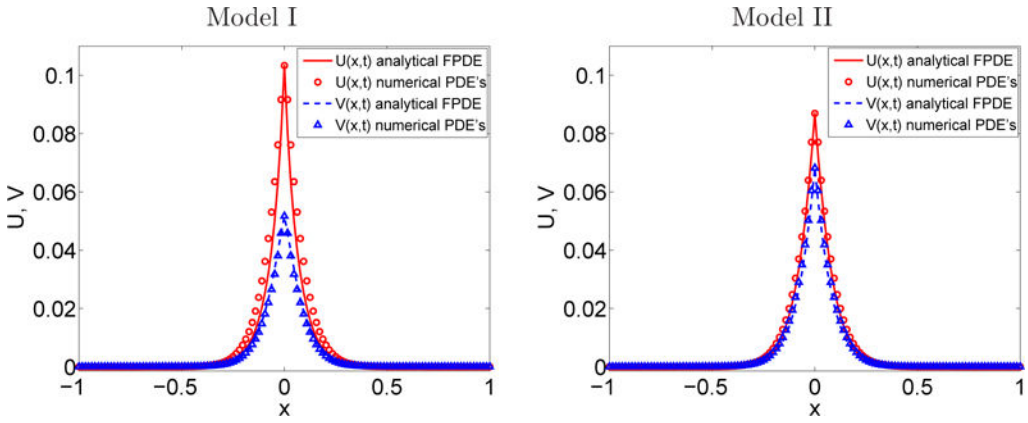

Fig. 5.6.

Section 5.5. Comparison between the numerical values (circles and triangles) and the analytical values (solid line and dashed line) of the concentration $U = \mathbf{e}^T \mathbf{u}$, $V = \mathbf{e}^T \mathbf{v}$ of A and B at time $t_1 = 10^{-2}$ s.

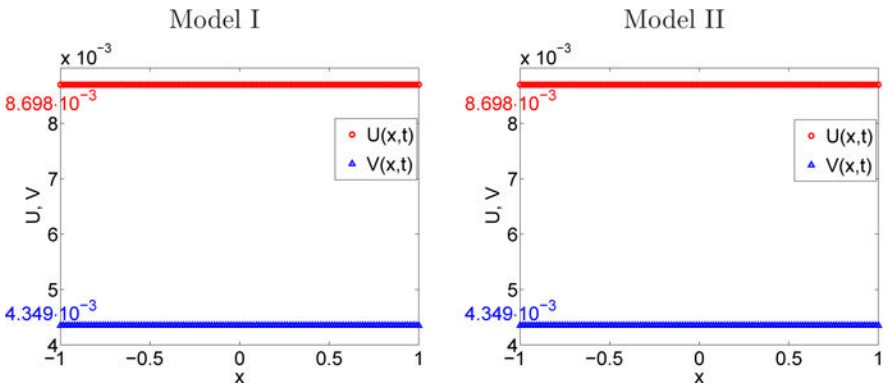

Fig. 5.7.

Section 5.5. Numerical values of the concentration $U = \mathbf{e}^T\mathbf{u}$, $V = \mathbf{e}^T\mathbf{v}$ of A and B at time $t_2 = 10$ s.

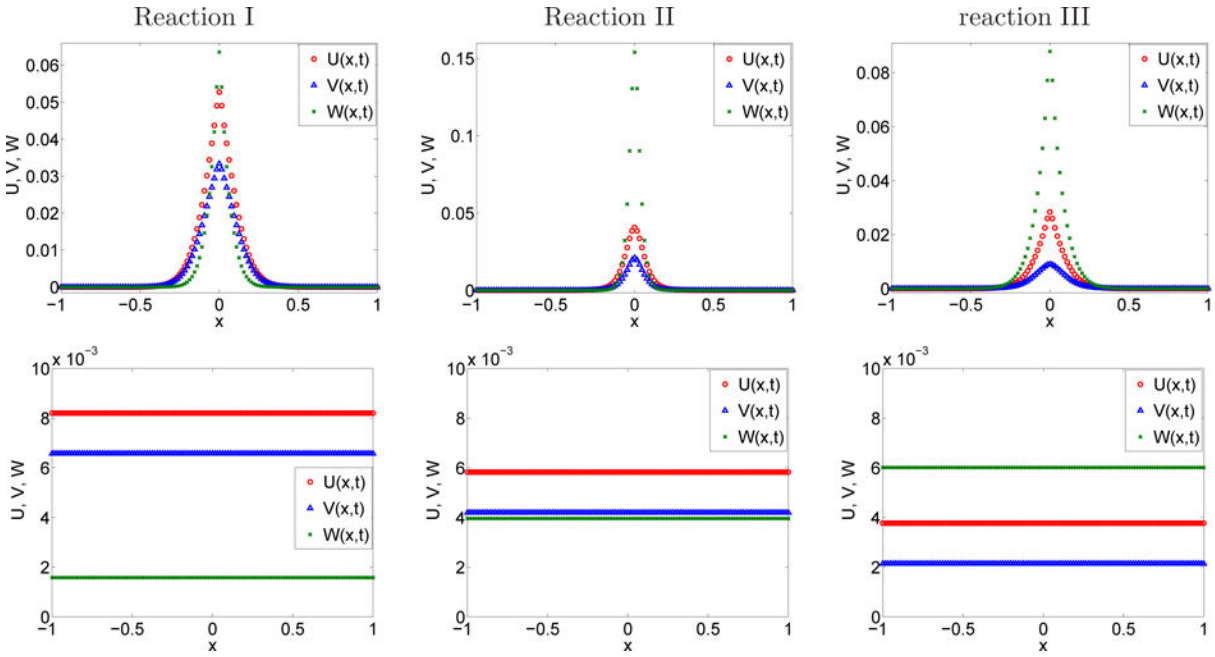

Fig. 5.8.

Section 5.6. Numerical values of the concentration $U = \mathbf{e}^T\mathbf{u}$, $V = \mathbf{e}^T\mathbf{v}$, $W = \mathbf{e}^T\mathbf{w}$ of A, B and C at time $t_1 = 1 \cdot 10^{-2}\ s$ (top) and $t_2 = 10\ s$ (bottom).

TABLE 3.1

Jump probabilities and propensities in (3.4) for different events.

	event	probability	propensity
Change of internal state	$A_j \to A_i$	$\pi_{ij} = \mu_i$	$a_j = y_j/\tau_j$
Diffusion from voxel k to voxel ℓ	$A_{jk} \to A_{j\ell}$	$\pi_{k\ell} = \lambda_{k\ell}/\lambda_k$	$a_j = \sigma_A^2 \lambda_k y_{jk}/\tau_j$
Monomolecular reaction	$A_j \to B_i$	$\pi_{ij} = \kappa_{ji}/\kappa_j$	$a_j = \kappa_j y_j/\tau_j$
Bimolecular reaction	$A_j \to B_i \to C_k$	$\pi_{ij} = \kappa_{ijk}/\kappa_{ij}$	$a_{ij} = \kappa_{ij} y_i z_j/\tau_{ij}$
Production of one molecule	$\varnothing \to A_i$	$\pi_{i0} = \mu_i$	$a_i = k/\tau_i$
Annihilation	$A_i \to \varnothing$	$\pi_{0i} = 1$	$a_i = k\, y_i/\tau_i$

Table 5.1

Parameters used in the numerical experiments.

	Parameters	Set 1	Set 2
Physical parameters	α	0.5	0.5
	K_α (m^2 s$^{-\alpha}$)	0.04	0.04
	t_{min} (s)	10^{-4}	10^{-3}
	t_{max} (s)	$5 \cdot 10^{-2}$	1
	σ^2 (m^2)	$3.49 \cdot 10^{-4}$	$7.18 \cdot 10^{-4}$
	τ (s)	$7.62 \cdot 10^{-5}$	$3.22 \cdot 10^{-4}$
Optimization	N	4	5
	τ_1 (s)	$9.51 \cdot 10^{-5}$	$7.58 \cdot 10^{-4}$
	τ_2 (s)	$5.40 \cdot 10^{-4}$	$3.55 \cdot 10^{-3}$
	τ_3 (s)	$3.09 \cdot 10^{-3}$	$1.66 \cdot 10^{-2}$
	τ_4 (s)	$2.13 \cdot 10^{-2}$	$7.89 \cdot 10^{-2}$
	τ_5 (s)	–	$4.78 \cdot 10^{-1}$
	μ_1	$4.96 \cdot 10^{-1}$	$3.23 \cdot 10^{-1}$
	μ_2	$2.07 \cdot 10^{-1}$	$1.48 \cdot 10^{-1}$
	μ_3	$8.80 \cdot 10^{-2}$	$6.84 \cdot 10^{-2}$
	μ_4	$4.42 \cdot 10^{-2}$	$3.24 \cdot 10^{-2}$
	μ_5	–	$1.85 \cdot 10^{-2}$
	ϵ_{mod}	$5.25 \cdot 10^{-2}$	$2.92 \cdot 10^{-2}$

Table 5.2

Reaction rates of annihilation process.

	First run		Second run	
	Model I	**Model II**	**Model I**	**Model II**
k	0.1	$8.727 \cdot 10^{-4}\ s^{-1}$	$5.729 \cdot 10^{-3}$	$50\ s^{-1}$
k_*	$8.727 \cdot 10^{-4}\ s^{-\alpha}$	$8.727 \cdot 10^{-4}\ s^{-1}$	$50\ s^{-\alpha}$	$50\ s^{-1}$

Table 5.3

Monomolecular reversible reaction. Reaction rates and theoretical steady state.

	Model I	**Model II**
k	$1.719 \cdot 10^3$	$15\ s^{-1}$
ℓ	$3.437 \cdot 10^3$	$30\ s^{-1}$
k_*	$15\ s^{-\alpha}$	$15\ s^{-1}$
ℓ_*	$30\ s^{-\alpha}$	$30\ s^{-1}$
u_∞ (mol m^{-1})	$8.698 \cdot 10^{-3}$	$8.698 \cdot 10^{-3}$
v_∞ (mol m^{-1})	$4.349 \cdot 10^{-3}$	$4.349 \cdot 10^{-3}$
k_{eq} (s^{-1})	$1.047 \cdot 10^6$	15
ℓ_{eq} (s^{-1})	$2.094 \cdot 10^6$	30

Table 5.4

Bimolecular reversible reaction. Reaction rates and theoretical steady states.

	Reaction I	**Reaction II**	**Reaction III**
k	37.5 m mol^{-1}	37.5 m mol^{-1}	7500 m mol^{-1} s^{-1}
ℓ	0.25	0.25	5 s^{-1}
u_∞ (mol m^{-1})	$8.204 \cdot 10^{-3}$	$5.826 \cdot 10^{-3}$	$3.772 \cdot 10^{-3}$
v_∞ (mol m^{-1})	$6.573 \cdot 10^{-3}$	$4.195 \cdot 10^{-3}$	$2.141 \cdot 10^{-3}$
w_∞ (mol m^{-1})	$1.582 \cdot 10^{-3}$	$3.959 \cdot 10^{-3}$	$6.014 \cdot 10^{-3}$
k_{eq} (m mol^{-1} s^{-1})	$2.450 \cdot 10^{3}$	$1.187 \cdot 10^{5}$	$2.483 \cdot 10^{1}$
ℓ_{eq} (s^{-1})	$8.351 \cdot 10^{1}$	$7.328 \cdot 10^{2}$	10^{2}